

The role of inherited extensional fault segmentation and linkage in contractional orogenesis: a reconstruction of Lower Cretaceous inverted rift basins in the Eastern Cordillera of Colombia

Andrés Mora,* Tatiana Gaona,† Jonas Kley,‡ Diana Montoya,† Mauricio Parra,* Luis Ignacio Quiroz,§ German Reyes† and Manfred R. Strecker*

*Institut für Geowissenschaften, Universität Potsdam, Golm, Germany

†Ingeominas, Bogotá, Colombia

‡Institut für Geowissenschaften, Universität Jena, Jena, Germany

§Smithsonian Tropical Research Institute, Balboa, Republic of Panamá

ABSTRACT

Lower Cretaceous early syn-rift facies along the eastern flank of the Eastern Cordillera of Colombia, their provenance, and structural context, reveal the complex interactions between Cretaceous extension, spatio-temporal trends in associated sedimentation, and subsequent inversion of the Cretaceous Guatiquía paleo-rift. South of 4°30'N lat, early syn-rift alluvial sequences in former extensional footwall areas were contemporaneous with fan-delta deposits in shallow marine environments in adjacent hanging-wall areas. In general, footwall erosion was more pronounced in the southern part of the paleorift. In contrast, early syn-rift sequences in former footwall areas in the northern rift sectors mainly comprise shallow marine supratidal sabkha to intertidal strata, whereas hanging-wall units display rapid transitions to open-sea shales. In comparison with the southern paleo-rift sector, fan-delta deposits in the north are scarce, and provenance suggests negligible footwall erosion. The southern graben segment had longer, and less numerous normal faults, whereas the northern graben segment was characterized by shorter, rectilinear faults. To the east, the graben system was bounded by major basin-margin faults with protracted activity and greater throw as compared with intrabasinal faults to the west. Intrabasinal structures grew through segment linkage and probably interacted kinematically with basin-margin faults. Basin-margin faults constitute a coherent fault system that was conditioned by pre-existing basement fabrics. Structural mapping, analysis of present-day topography, and balanced cross sections indicate that positive inversion of extensional structures was focused along basin-bounding faults, whereas intrabasinal faults remained unaffected and were passively transported by motion along the basin-bounding faults. Thus, zones of maximum subsidence in extension accommodated maximum elevation in contraction, and former topographic highs remained as elevated areas. This documents the role of basin-bounding faults as multiphased, long-lived features conditioned by basement discontinuities. Inversion of basin-bounding faults was more efficient in the southern than in the northern graben segment, possibly documenting the inheritance and pivotal role of fault-displacement gradients. Our observations highlight similarities between inversion features in orogenic belts and intra-plate basins, emphasizing the importance of the observed phenomena as predictive tools in the spatiotemporal analysis of inversion histories in orogens, as well as in hydrocarbon and mineral deposits exploration.

INTRODUCTION

A better understanding of the processes and styles governing the inversion of inherited normal faults in orogenic

belts is a fundamental problem in structural geology. For example, in orogens the presence of structural and stratigraphic traps related to former rift tectonics may guide the migration of fossil fuels and the emplacement of mineral resources (e.g. Uliana *et al.*, 1995). In such settings, the origin and evolution of inverted structures are therefore important in improving exploration. Furthermore, if pronounced pre-existent anisotropies related to extensional

Correspondence: Andrés Mora, Institut für Geowissenschaften, Universität Potsdam, Karl Liebknecht-Str 24, D14476 Potsdam-Golm, Germany. E-mail: andres.mora@geo.uni-potsdam.de

tectonics are favorably oriented with respect to the greatest horizontal stress during a subsequent contractile phase, reactivation of such structures may significantly impact the spatiotemporal evolution of deformation in the entire mountain belt (e.g. Lowell, 1995). Hence the width of an orogen may be a direct consequence of this type of interaction and its growth may not be governed by the principles of wedge mechanics (e.g. Davis *et al.*, 1983) documented in regions where such inherited structures do not exist (Hilley *et al.*, 2005). In addition, the polarity of normal faults, associated disparities in syntectonic sediment thickness, and existence of extensional transfer structures may exert an important control on orogenic evolution during contraction (e.g. Hayward & Graham, 1989).

Positive basin inversion involves the partial or total reversal of motion on extensional faults subjected to superimposed compressional stresses (Williams *et al.*, 1989). The phenomenon of basin inversion has been documented worldwide. For example, mild to moderate inversion in intraplate basins has been observed in numerous North Atlantic basins (Cartwright, 1989; Chapman, 1989; Hayward & Graham, 1989; Roberts *et al.*, 1993; Sinclair, 1995; Thomas & Coward, 1995) or in the North German Basin (Kossov *et al.*, 2000; Kossov & Krawczyk, 2002; Gemmer *et al.*, 2003). In addition, strongly shortened half grabens have been documented in the Alps (Gillcrisp *et al.*, 1987), with prominent examples found in the Central Andes (Kley & Monaldi, 2002) and Atlas mountains (Beauchamp *et al.*, 1999; Teixell *et al.*, 2003).

Huyghe & Mugnier (1995) suggested that the nature of inversion in mildly inverted intraplate basins is different from inversion in orogenic belts where extensional structures are typically fully reversed, creating topography and exposure of former basin strata (e.g. Badley, 2001). The time span between the extensional phase and the onset of subsequent contraction is often larger in orogenic belts compared with intraplate basins (Huyghe & Mugnier, 1995). Therefore, by the time a formerly rifted lithosphere undergoes contraction in an orogenic setting, it may have recovered its pre-extensional strength (Huyghe & Mugnier, 1995). In this context, it is an important question if different crustal properties influence variations in inversion styles in fully developed orogenic belts in comparison with intraplate basins.

In intraplate basins undergoing mild to moderate inversion, high-quality seismic images have improved our 3D understanding of the behavior of individual normal faults and linked graben systems during subsequent compression (Cartwright, 1989; Chapman, 1989). Furthermore, laboratory 3D analog models of inversion have helped visualize the first-order principles and structures associated with these processes (Eisenstadt & Withjack, 1995; McClay, 1995).

In the more severely inverted basins of many orogens, however, detailed field-based accounts regarding the mechanical interaction of segmented former extensional faults, the nature of displacement transfer, and how such structures are incorporated into the orogenic realm are

rare (Hayward & Graham, 1989; García Senz, 2002; Kley *et al.*, 2005; Monaldi *et al.*, 2008). These problems are often compounded by a general lack of good seismic images with unequivocal extensional features. Furthermore, due to the high degree of superimposed shortening, a precise assessment of extensional features is made difficult at the outcrop level, as in the case of the Western Alps (e.g. Gillcrisp *et al.*, 1987; Coward *et al.*, 1989; Graciansky *et al.*, 1989; Hayward & Graham, 1989). In these extreme cases, a palinspastic reconstruction may help decipher the principal extensional features and original location of ancestral extensional structures (e.g. Nemcok *et al.*, 2001). Finally, prominent along-strike changes in the patterns and styles of deformation have been observed in many inversion orogens (Grier *et al.*, 1991; Carrera *et al.*, 2006). However, few studies have unambiguously demonstrated that those changes are indeed determined by along-strike variations in the modes of previous extensional deformation, fault interaction, and linkage.

The Eastern Cordillera of Colombia (Fig. 1) has experienced much less deformation than many other inversion orogens (e.g. Colletta *et al.*, 1990; Mora *et al.*, 2006). It therefore has the advantage of furnishing valuable information on ancient normal fault arrays, the characteristics of associated syn-rift depositional settings, and the lateral evolution before contraction.

In this study, we document a previously unrecognized pattern of extensional fault interaction, deduced mainly from early syn-rift stratigraphic sequences associated with former normal faults. First, we determine the local characteristics and lateral extent of syn-rift units in light of the Early Cretaceous paleotopography in order to use the sedimentary facies associations as proxies for past normal fault evolution and linkage. Second, we evaluate the effects of the pre-existing extensional fault arrays on Cenozoic contractional deformation. In contrast with the study of Mora *et al.* (2006), we use sedimentology to document that a pattern of selective fault reactivation is not only due to the orientation of the compressive stress field with respect to the pre-existent faults (Mora *et al.*, 2006), but is also related with the pattern of extensional fault growth.

GEOLOGIC SETTING OF THE EASTERN CORDILLERA

The Colombian Eastern Cordillera is an atypical Andean foreland fold and thrust belt. In stark contrast with other Andean foreland fold and thrust belts it appears to be more influenced by inherited structures rather than subduction related orogenesis (e.g. Colletta *et al.*, 1990). The spatial coincidence between the Eastern Cordillera (Fig. 1) and a Neocomian extensional province was proposed by Colletta *et al.* (1990), although it has also been suggested that this region may represent a simple ramp basin that subsided more than adjacent regions during the Early Cretaceous (Roeder & Chamberlain, 1995), similar to the Cameros Basin in northern Spain (Guimera *et al.*, 1995). Indeed, in

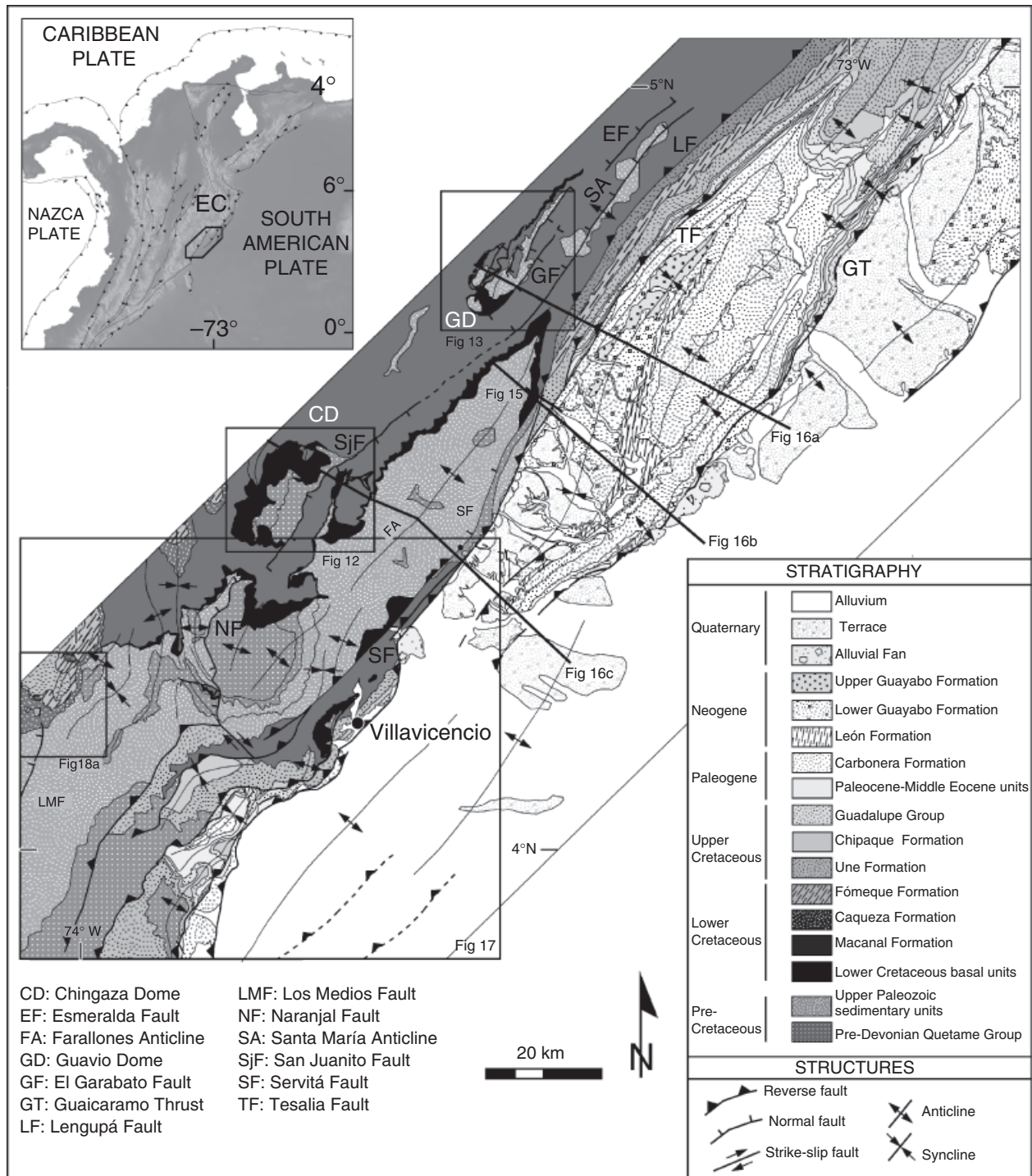


Fig. 1. (a) Geodynamic setting and simplified topography of the northern Andes. The study area is indicated by the box. (b) Geological map of the Farallones de Medina area with location of the cross sections in Fig. 15. Map depicts areas covered in Figs 12, 13, 17, 18 and locations of balanced structural profiles.

the Eastern Cordillera it had been impossible to recognize and precisely locate former rift-controlling faults. However, basin-analysis studies of this region favor a rift model (Sarmiento-Rojas *et al.*, 2006). In addition, structural reconstructions (Mora *et al.*, 2006) unambiguously show that the Early Cretaceous basin along the eastern flank of the Eastern Cordillera was a rift zone. These authors proposed a reactivation mechanism restricted to an in-

verted frontal master fault (Servitá fault), where the entire eastern flank of the EC was passively uplifted while the internal structures underwent virtually no contractile reactivation. The main reason for selective fault reactivation in the Cretaceous extensional province was inferred to be related to the orientation of the tectonic stress field with respect to the pre-existing anisotropies (Mora *et al.*, 2006).

The investigated area of this study is located in the Farallones de Medina range of the Eastern Cordillera. This area (Figs 1 and 2) is located along the eastern foothills of the mountain belt and exposes lower Cretaceous syn-rift facies in different tectonic blocks. Although the structural relationships in this region are now well known (e.g. Mora *et al.*, 2006), the lateral distribution of syn-rift facies and their relationship to the structures is not yet fully understood.

Phyllites and green schists of the pre-Devonian Quechame Group constitute the oldest rocks in the area and are overlain by the sedimentary Farallones Group. These units comprise Devonian nonmarine to shallow marine sandstones (Areniscas de Gutierrez Formation); Carboniferous continental red-bed sequences (Capas del Valle del Guatiquía Formation), and Permian shallow marine carbonates (Gachalá Formation).

The upper Paleozoic rocks are superseded by *ca.* 5-km-thick Cretaceous sequence (Fig. 3). The lowermost Berriasian and Valanginian units overlying the Paleozoic rocks are the main target units of this study, as they represent the early syn-rift strata. However, the Berriasian strata cannot be grouped into one single, basal lithostratigraphic unit as these strata display rapid lateral facies changes. For example, calcareous units overlying the pre-Cretaceous basement have been grouped into the Calizas del Guavio Formation (Ulloa & Rodríguez, 1979); coeval strata composed of polymictic gravels, breccias, fluvial sandstones and associated overbank fines constitute the Brechas de Buenavista Formation (Dorado, 1992). In other locations, shallow marine terrigenous lithic sandstones, polymictic conglomerates, and subordinate amounts of gray siltstones of Early Cretaceous age that overly Paleozoic rocks belong to the Batá Formation (Bürgl, 1961; Geyer, 1973; Ulloa & Rodríguez, 1979; Etayo-Serna *et al.*, 2003, Fig. 2). All of these units are therefore lateral equivalents and are overlain by an ammonite-dominated shale unit (Lutitas de Macanal Formation, Fig. 2).

METHODS

Our study focuses on Berriasian and Valanginian strata recording the earliest syn-rift sedimentation in the Farallones de Medina area. We produced a field structural map of the study area based on 1 : 25 000 and 1 : 10 000 topographic maps and aerial photographs (Fig. 1). Careful field structural mapping helped detect and define the best exposures of the early syn-rift units. Where possible, we chose profiles displaying well exposed contacts with the underlying Paleozoic substratum and used this unconformity as a marker horizon. We measured detailed (1 : 200) stratigraphic columns using a Jacob staff. In the gravel intervals, we analyzed clast compositions in order to determine provenance (Table 1). Additional quantitative petrologic data is mostly absent in those non-conglomeratic intervals. Paleocurrent measurements of groove casts were mainly taken in turbiditic sandstone strata. However, paleocurrent data is scarce in most of the localities. In addition, we integrated our data with published sec-

tions (Stibane, 1968; Dorado, 1992; Parra, 2000; Geostratos, 2005; Rincón & Tamara, 2005). The measured sections (Fig. 3) were described according to 10 different facies associations. The graphic symbols in the profiles, representing various lithologic and primary features observed in the field and reported in our stratigraphic profiles can be seen in Fig. 4. Sections were correlated by following key horizons in the field or on aerial photographs based on prominent topographic features. Using these data, we constructed a map of early syn-rift facies with the interpreted sedimentary environments in this extensional setting during the Early Cretaceous. To expand our analysis of superimposed contractional deformation, we also constructed three balanced cross sections based on outcrop and seismic data.

SEDIMENTARY CHARACTERISTICS OF THE EARLY CRETACEOUS RIFT-BASIN FILL

Buenavista formation

Facies association B1

This facies association constitutes the basal conglomerate at localities 5, 6, 7 (Fig. 6) 11, 12 (Fig. 7) and 16, and most of the sequence at localities 1 and 2 (Fig. 5). Its thickness typically ranges from 10 to 40 m. This association is characterized by a set of very thick beds, either with lenticular geometry or irregular geometry, occasionally lacking internal stratification. The individual beds are composed of poorly sorted cobble-sized, subrounded conglomerates (in localities 5, 11 and 12 some 25–60 cm boulders are also present), mostly supported by a sandy to silty matrix. The cobble-size fraction is predominantly monomictic quartzose. Sorting is commonly poor. Often, there are interbedded pebble-conglomerates and pebbly conglomeratic sandstones in well-defined beds with variable thickness and inverse grading.

We interpret these rocks to have been deposited in an alluvial-fan system. Matrix-supported conglomeratic beds with sandy matrix and irregular geometry may correspond to debris-flow deposits, whereas conglomeratic beds with well-defined geometry reflect confined channel flows during stream-dominated deposition (e.g. Rust & Koster, 1984; Nemeč & Postma, 1993). At locality 1 (Fig. 5), there is a clear lateral change toward marine facies (i.e. black shales with ammonites) suggesting that in some localities these conglomeratic beds are transitional between fluvial and coastal environments.

Facies association B2

This facies association is characterized by poorly sorted breccias and coarse matrix-supported conglomerates lacking internal organization or well defined bedding surfaces. This facies association is a lateral equivalent of shallow marine units because it normally outcrops adjacent to ammonite bearing black shales. The thickness is highly

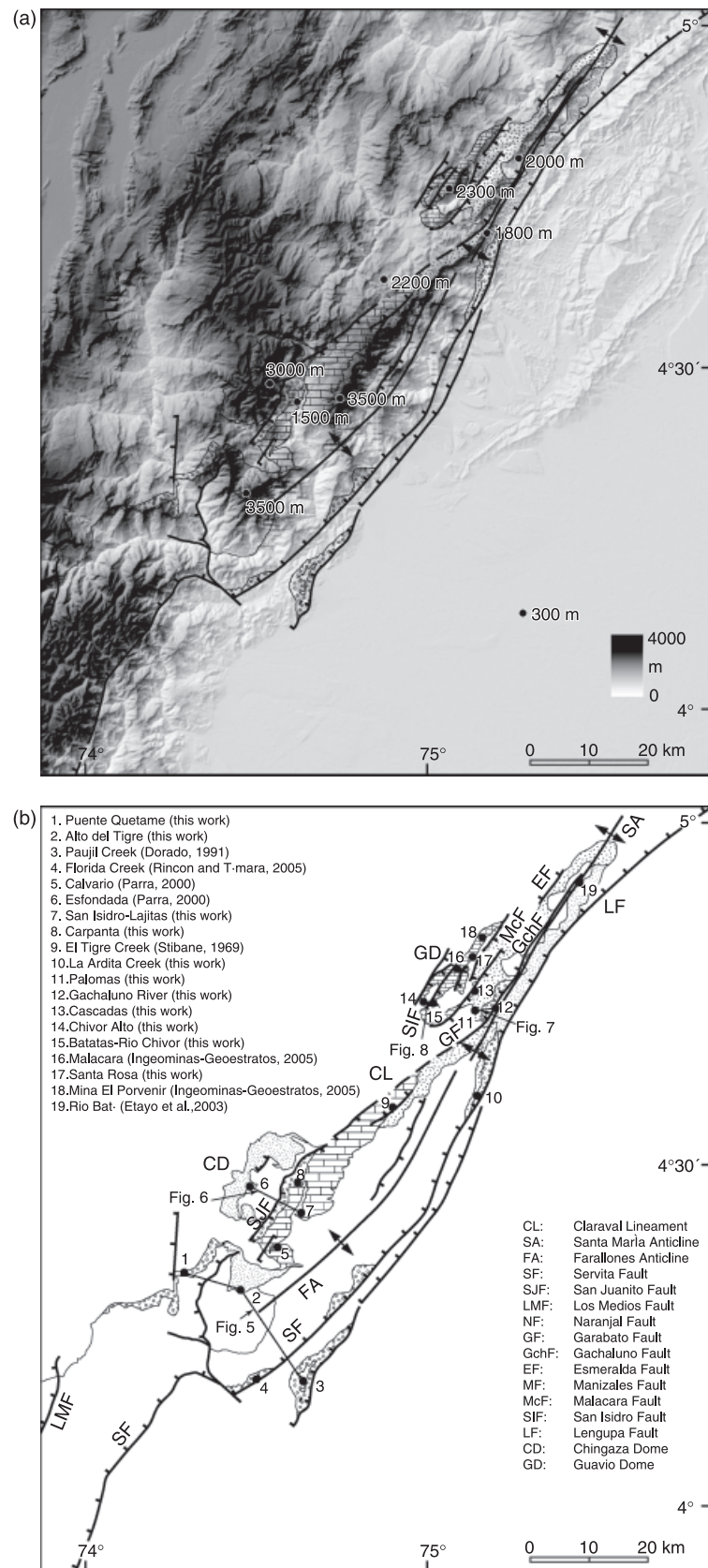


Fig. 2. (a) Reconstructed distribution of Early Cretaceous faults. The numbers are elevations above sea level in certain localities. (b) Locations of the stratigraphic sections quoted in the text.

Table 1. Clast count method

Section/m above base	Composition of fragments	
	Sedimentary rocks	Unstable-basement rocks
1. Puente Quetame		
68	100	0
70	100	0
61	100	0
48	100	0
25	100	0
19	100	0
16	100	0
2. Alto del Tigre		
437	100	0
426	100	0
415	100	0
405	17	83
387	24	76
363	57	43
354	52	48
263	67	33
137	71	29
24	56	44
13	100	0
3. Paujil		
Lower segment	< 30	> 70
Upper segment	65	35
4. Florida Creek	> 50	Observed
5. Calvario		
2	100	0
6. La Esfondada		
6	100	0
5 (*)	45	55
7. San Isidro-Lajitas		
525	71	29
523	89	11
515	62	38
503	57	43
497	68	32
484	97	3
447	85	15
422	74	26
1	100	0
8. Carpanta		
118	53	47
90	87	13
45	64	34
17	95	5
9. El Tigre Creek		
10. La Ardita Creek		
248	100	0
224	100	0
195	100	0
164	100	0
142	100	0
118	100	0
102	100	0

Table 1. (Continued)

Section/m above base	Composition of fragments	
	Sedimentary rocks	Unstable-basement rocks
72	100	0
29	92	8
24	90	10
18	80	20
11. Palomas		
12	100	0
15	100	0
18	100	0
12. Gachaluno River		
14	100	0
9	100	0
73	100	0
55	100	0
159	100	0
13. Cascadas		
14. Chivor Alto		
15. Batatas		
59	100	0
43	100	0
18	100	0
10	100	0
16. Malacara		
17. Santa Rosa		
18. Mina El Porvenir		

After a general inspection of the outcrop and rough analysis of the clasts present, an arbitrary face was selected in order to count the composition of the clasts in every single gravel size grain (up to boulder size). The fractions were separated in clasts of sedimentary rocks, milky quartz from veins, feldespars (never found) and unstable or clearly discernible basement lithologies. We took in this table the sedimentary clasts plus the basement rocks as 100. Then put in the table the amount of each fraction with respect to the total. Our goal was only to detect the presence or absence of basement rocks.

variable and the lateral continuity is restricted. This facies association overlies the basal Cretaceous unconformity at localities 3 (Fig. 5), 2, 8, 10 and 15 (Fig. 8), and at about 375 m above this unconformity, at locality 7 (Fig. 6). Typically, this facies consists of boulders (> 60 cm in diameter) and cobbles in a pebbly to sandy matrix. Some boulders exceed 2 m in diameter; angular to sub-angular clasts dominate. Owing to a general lack of organization and a high fraction of metamorphic basement clasts this facies association differs from the basal conglomerates in facies association B1 (Table 1, Quetame Group phyllites), except at outcrop locality 10, where these clasts are virtually absent.

Owing to the poor stratification and sorting, abundant angular fragments, and limited lateral continuity, the matrix-supported conglomerates of facies association B2 are interpreted as debris flow deposits (Rust & Koster, 1984; Nemeč & Postma, 1993; Blair & McPherson, 1998). The rapid lateral transition into marine facies (e.g. facies

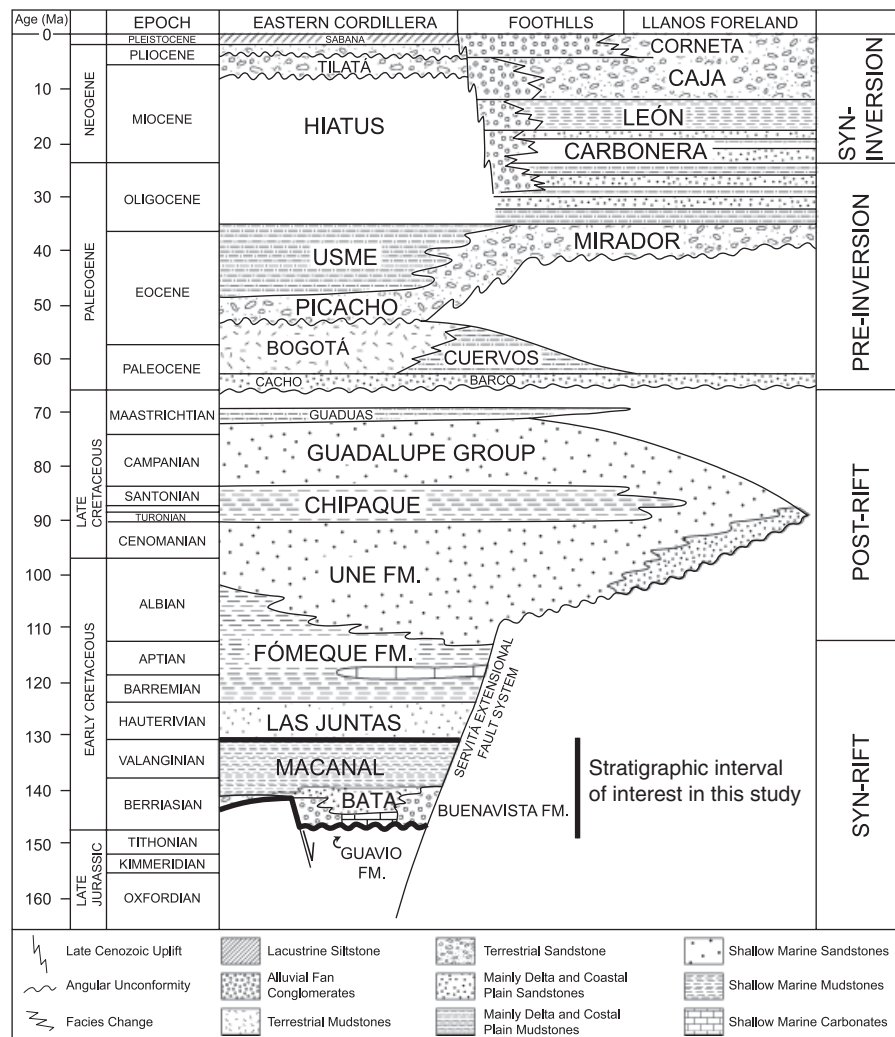


Fig. 3. Meso-Cenozoic stratigraphy of the eastern flank of the Eastern Cordillera with the stratigraphic interval of interest highlighted (Modified from Mora *et al.*, 2006).

associations M1) indicates a fan delta in a shallow marine setting.

Facies association B3

These units comprise tabular to lenticular beds, 0.3 to several meters thick, with medium- to coarse-grained lithic sandstones and laterally equivalent lithic conglomeratic sandstones and conglomerates. Medium to thick beds (up to 1 m thick) of siltstones and mudstones are interbedded with the upper sandstones of this facies association. It is well developed at localities 2 (intervals between 30 and 83 m and, between 325 and 383 m, Fig. 5) and 6 (lower segment of the basal syn-rift unit, Fig. 6). The lower 40 m at locality 6 (Fig. 6) have a ratio of sand to mud layers of about 90 : 10. Amalgamated sandstone beds with lenticular geometry are abundant, with frequent inverse grading and occasionally with planar cross bedding. However, in the upper 150 m at locality 6 the sand to mud layer ratio is 40 : 60. This section contains frequent thin to very thick-bedded (*sensu* Ingram, 1954) red-colored siltstones to sandy

siltstones with pervasive mottling. These are interbedded with medium to thick-bedded lithic sandstones (petrography after Parra, 2000) with normal grading and channel geometry. Amalgamated sandstone beds very often display lateral accretion surfaces and have thin basal conglomeratic lags.


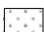
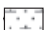





The amalgamated lithic sandstone beds in the lower 40 m at locality 6 and 2 are interpreted as bars in a braided river system (e.g. Collinson, 1996; Miall, 1996). In the upper 150 m of locality 6, the channelized sandy fining-upward sequences with lateral accretion surfaces suggest a meandering river environment. Accordingly, interbedded siltstones and sandy siltstone beds with pervasive mottling represent floodplain deposits and overbank fines (Miall, 1985).

Calizas Del Guavio formation












Facies association C1

Facies association C1 is well developed at localities 18 (between 160 and 215 m), 15 (between 95 and 160 m) and 14

SILICICLASTIC SEDIMENTARY ROCKS

	Breccia
	Conglomerate
	Conglomeratic sandstone
	Sandstone
	Calcareous sandstone
	Muddy sandstone
	Siltstone
	Sandy mudstone
	Claystone
	Shale
	Red mudstone

CARBONATE SEDIMENTARY ROCKS

	Limestone
	Dolomite
	Stromatolites with laminated fabric
	Stromatolites with hemispheroidal fabric
	Sandy limestone
	Muddy limestone
	Marlstone
	Evaporite pseudomorphs with nodular fabric
	Micrite interlayering
	Pyrite laminae
	Pyrite nodules
	Evaporite pseudomorphs with enterolithic structures
	Calcareous concretions
	Chickenwire structures






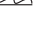



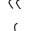
















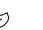



	Parallel lamination
	Continuous wavy bedding
	Discontinuous wavy bedding
	Lenticular bedding
	Flaser bedding
	Trough cross bedding
	Ripples
	Planar cross bedding
	Planar cross bedding with tangential foresets
	Crude bedding
	Bioturbation
	Rootlets
	Synsedimentary folding
	Slumps
	Imbrication
	Erosion surface
	Groove cast
	Inverse grading
	Normal grading
	Angular unconformity
	Bivalves
	Gastropods
	Ammonites
	Foraminifera
	Brachiopods
	Crinoids
	Corals
	Echinoderms
	Plant remains
	Trunk remains
MO	Organic matter
Y	Gypsum
	Fault

Fig. 4. List of symbols and abbreviations and their meaning. These symbols and abbreviations were used in Figs 5, 6, 7, 8, and 10.

(discontinuous interval between 35 and 135 m Figs 2 and 8), and it consists of two distinct interfingering cycles with a thickness of 0.5–2 m. First, laminated dolomitic mudstones (at locality 15) or laminated calcareous mudstones (at localities 14 and 18) alternate with thin- to medium-bedded nodular calcareous mudstones, often with chicken-wire growths, enterolithic folding, and fenestrae. Desiccation cracks occur on top of some of the beds in this unit. The second unit comprises laminated structures interpreted to be stromatolites (Kalkowsky, 1908; Logan

et al., 1964; Tucker & Wright, 1990; Riding, 2000). In addition, we found a clothed texture reflecting syn-depositional processes at locality 15, also interpreted to reflect microbial origin (strombolites *sensu* Riding, 2000). At localities 18 and 15a these associations are also interbedded with very thick black shale and black marl horizons, occasionally with laminae rich in pyrite.

The first unit is characteristic of evaporite pseudomorphs. For example, nodules and enterolithic structures (Fig. 9) resemble diagenetic structures formed in modern

W

E

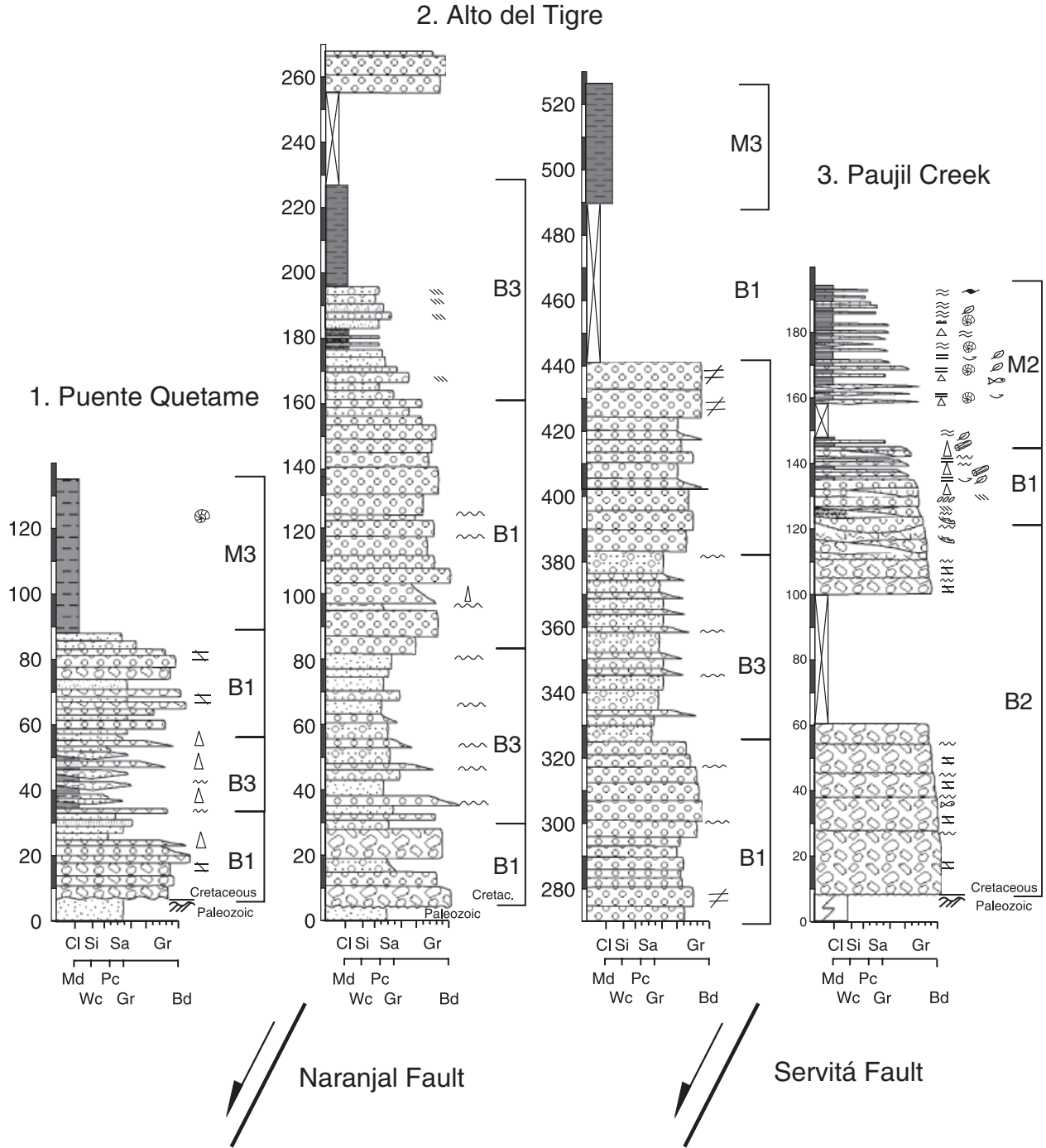


Fig. 5. See locations in Fig. 2. Stratigraphic logs located in the southernmost segment of the study area. Contrasting facies in the different profiles coincides with different faulted domains.

anhydrites (Kendall & Harwood, 1996; Alsharhan & Kendall, 2003). Alternations of dolomitic mudstones and anhydrite are common under hypersaline conditions when calcium sulfate precipitates and residual waters are enriched in magnesium (Alsharhan & Kendall, 2003). Facies association Cl thus suggests deposition under conditions typical of coastal sabkhas (Warren & Kendall, 1985; Alsharhan & Kendall, 2003). In combination with the desiccation

cracks, these characteristics reflect arid to hyperarid climate conditions (Tucker & Wright, 1990).

The second, stromatolite-bearing unit is interpreted to indicate a temporary changeover from supratidal sabka to intertidal conditions, similar to present-day environments reported in Dubai (Tucker & Wright, 1990). The presence of black shales and marls interbedded with the other units suggests subtidal conditions, possibly associated

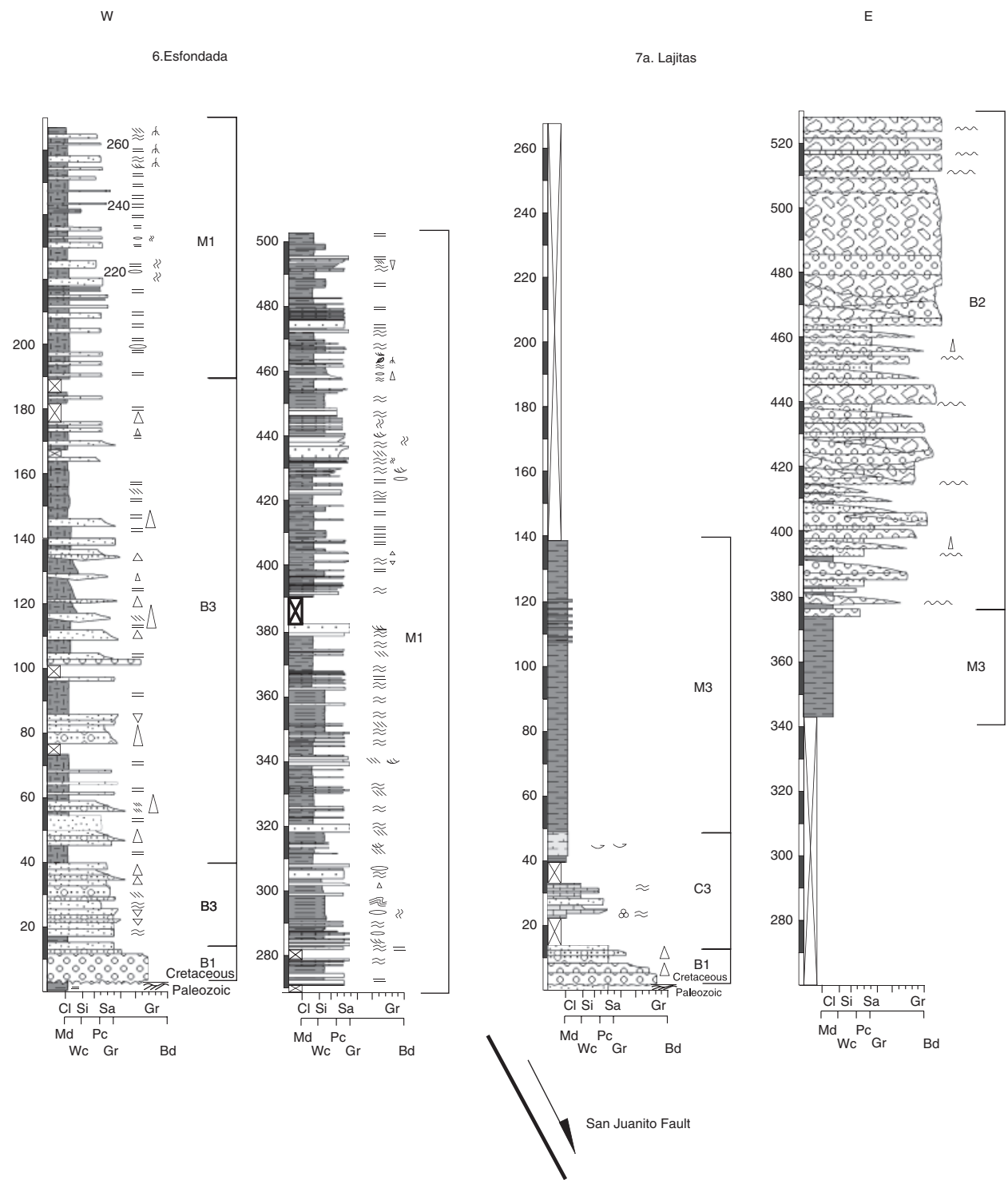


Fig. 6. See locations in Fig. 2. Stratigraphic profiles in the footwall and hanging wall blocks of the San Juanito fault depicting marked contrasts between early syn-rift facies in both domains.

with an euxinic basin. Overall, these deposits appear to indicate oscillating sea level in a sustained arid environment.

Facies association C2

This facies association is characterized by tabular beds of mudstones, marls, and intraclastic wackestones, well developed at locality 15c (Fig. 8, between 0 and 95 m). The

beds commonly contain disseminated bivalve shells (bioclastic wackestones). Locally bivalve packstones are found. In this facies association, well-sorted bioclasts generally do not occur in growth position and are sub-horizontal with respect to bedding. Occasionally, poorly sorted bioclasts are found in different positions.

We interpret this facies association to be related to internal to intermediate parts of a carbonate platform enviro-

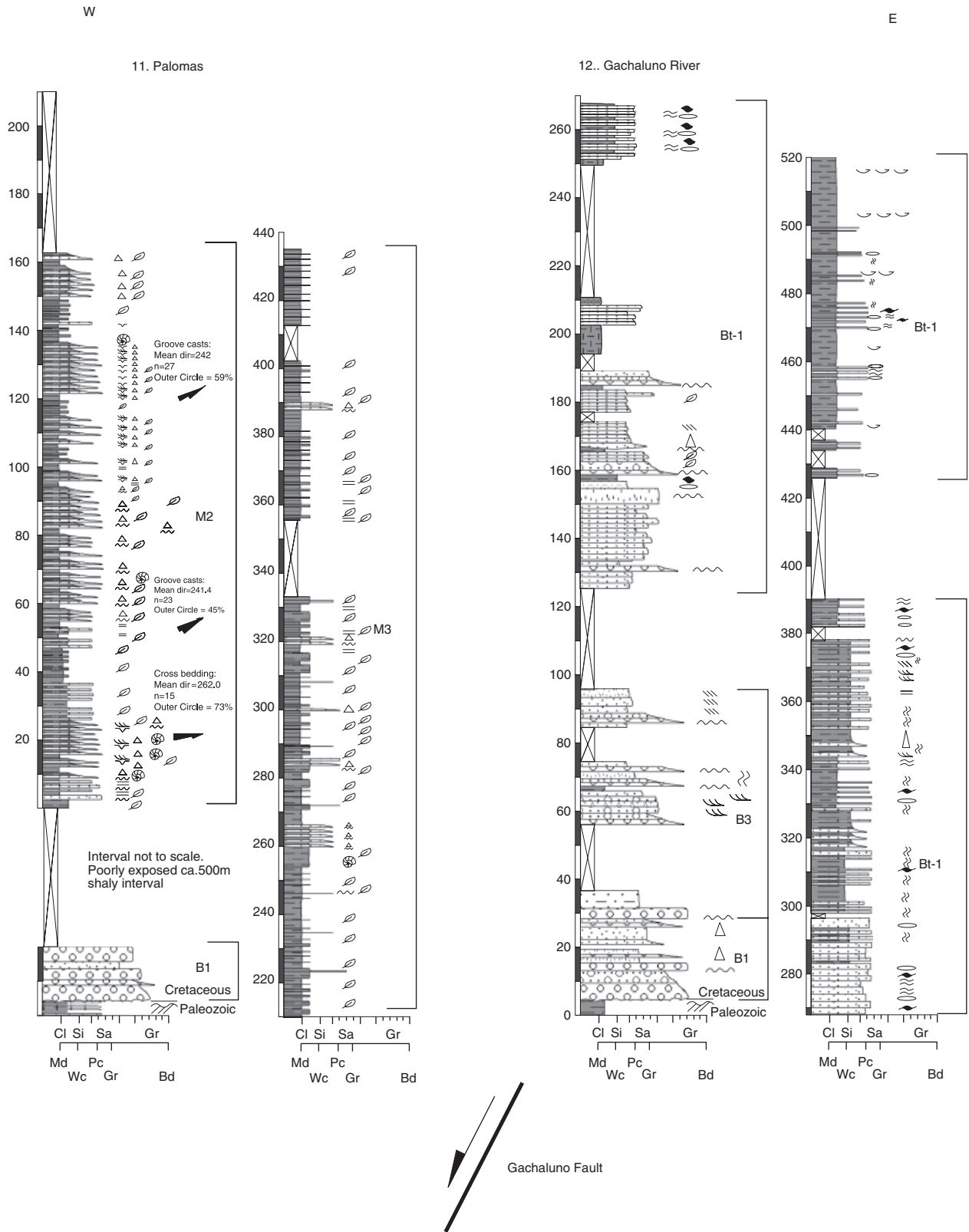


Fig. 7. See locations in Fig. 2. Stratigraphic logs east and west of the Gachaluno fault showing different early syn-rift facies in each domain controlled by the Gachaluno fault.

onment. Abundant wackestones and some bioclastic packstones with horizontal, well-sorted, and often disarticulated bivalves may correspond to proximal storm-flow shell concentrations (*sensu* Fürsich, 1995). In contrast, the

less frequent wacke- and packstone levels with rarely broken, often articulated bivalve shells in different positions, and poor selection, may indicate storm-wave action (storm wave shell concentration *sensu* Fürsich, 1995). Overall, we

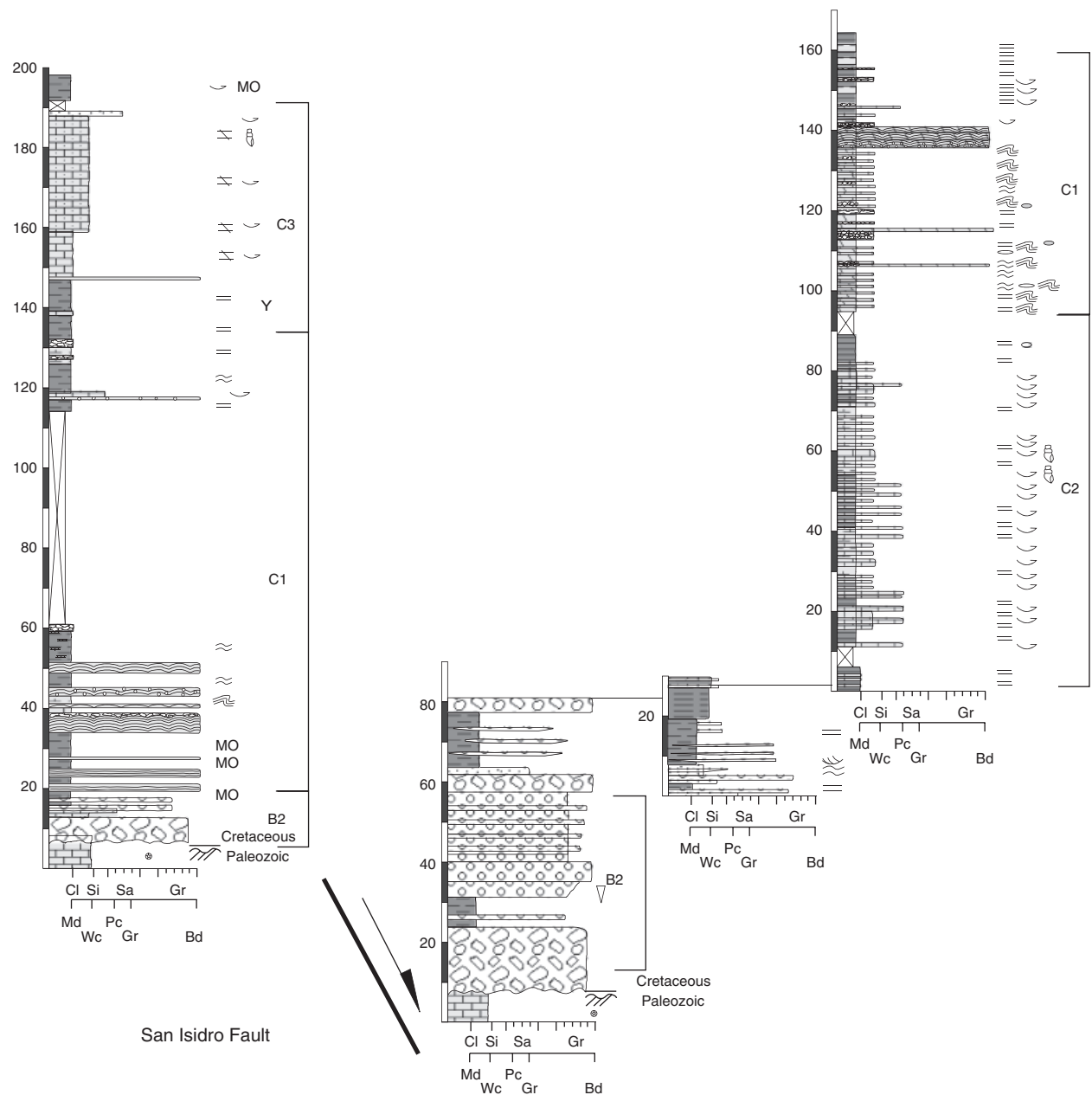


Fig. 8. See locations in Fig. 2. Early syn-rift facies controlled by the San Isidro fault, northern segment of the study area.

interpret the tabular wacke- and mudstone layers to have been deposited above the basal level of storm influence and below the basal level of fair-weather wave influence.

Facies association C3

Tabular beds of quartzose wackestones, calcarenites, carbonate-cemented sandstones, and minor calcareous mudstones characterize this facies association. The C3 facies association occurs at locality 14 (between 145 and 190 m, Fig. 8) and in lower non-conglomeratic segments of locality 7a and 7b (Figs 2 and 6). Interestingly, at both localities there are occasional horizons where the bulk of the rock is composed of calcareous mudstone but most of the

sand-size components consisting of quartz or terrigenous fragments (petrography after Parra, 2000). At locality 7a, Parra (2000) observed bioclasts of agglutinated benthic foraminifera (*Textularia* sp., *Glomospira* sp.), a minor amount of planktonic species (*Praeglobulina* sp.), and ostracods. In addition, gastropods occur in the lowermost calcareous beds at locality 7b.

The coarser grain size of this facies association represents a higher-energy version of facies association C2. We interpret the C3 association as internal carbonate platform deposits. In addition, the presence of quartz and other terrigenous components indicates an adjacent terrigenous sediment source. Ostracods, agglutinated foraminifera, and gastropods may indicate a restricted, probably high salinity, internal platform environment.

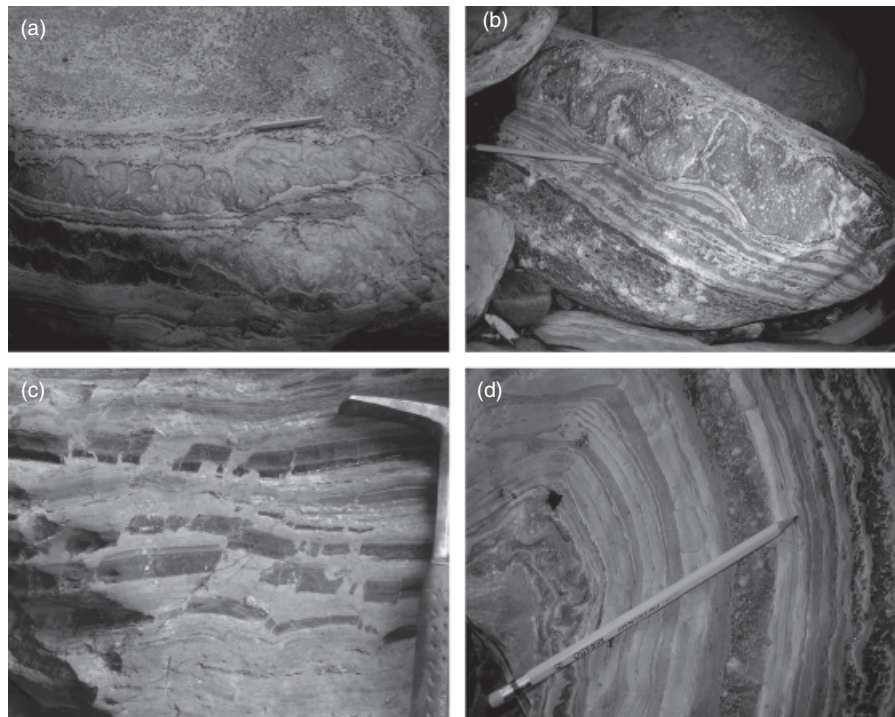


Fig. 9. Photographs of facies association C1 at locality 15. (a) Enterolithic structures interlayered in a laminated sequence of dolomites and mudstones. (b) Detail of enterolithic structure above interlamination of dolomites and mudstones. Notice below the laminated beds the presence of calcite nodular growths (anhydrite pseudomorphs?). (c) Interlamination of dolomites (light layers) and mudstones (dark layers) of interpreted microbial origin. (d) From left to right. Small enterolithic growths; first laminated dolomites; layer with abundant nodular growth; second laminated dolomites.

Batá formation

Facies association Bt-1

Facies association Bt-1 is well represented at localities 12 and 19. It constitutes a continuously exposed horizon between both localities. The lower section in locality 12 overlying Paleozoic rocks consists of a 30-m-thick conglomerate included in facies association B1. This unit is overlain by *ca.* 70 m of strata corresponding to facies association B3. This interval is superseded by a *ca.* 400-m-thick sandstone unit that constitutes facies association Bt-1 (Fig. 7). The dominant lithology consists of amalgamated medium to thick beds of medium- to coarse-grained quartz sandstones. These layers are often interbedded with thin, fine-grained sandstones exhibiting flaser and lenticular bedding. Occasionally, bioturbation (burrows) characterizes these beds. The medium to thick quartz-sandstone layers are commonly interbedded with upward fining, very thick to massive lithic to sub-lithic sandy to conglomeratic layers with erosional bases marked by conglomeratic lags. Large-scale cross bedding with conglomeratic laminae often accompanies layers exhibiting erosional bases. These strata are well developed between 30 and 190 m at locality 12 (Fig. 7).

At this location, the upper stratigraphic horizons of this facies association are characterized by decreasing sandstone, absence of upward fining conglomeratic sandstone layers, and an increasing proportion of interbedded mud- and siltstones. Between 290 and 360 m, transitions between muddy and sandy

facies are commonly bioturbated (burrows) and flaser, lenticular, and wavy laminations are typical. However, these features are less common in the upper portion of the facies association above 360 m, which is a dominantly muddy interval.

The lower monomineralic sandstones with interbedded thin fine-grained sand to siltstone layers with flaser bedding are interpreted as shoreline deposits (Galloway & Hobday, 1996; Reading & Collinson, 1996). However, the lithic sandstones and fine-grained conglomerates with sharp basal contacts and fining-upward sequences indicate a periodic influence of fluvial processes in this near-shore environment (Dalrymple & Choi, 2007). In this context, the large-scale cross bedding with conglomeratic laminae may correspond to fluvial lateral accretion surfaces. We suggest that this fluvial influence disappears progressively upsection as lithic sandstones and conglomerates with fining upward sequences disappear. In the upper part of this facies association, an increasing proportion of shales and siltstones, a decreasing sandstone granulometry, and the presence of bioturbated intervals suggest a middle to lower shoreface environment (Galloway & Hobday, 1996).

Macanal formation

Facies association M1

This association is characterized by laminated beds of variable thickness with sandy mudstones, siltstones, and fine-grained sandstones that are exposed over a *ca.* 300 m interval in the upper section of the profile at locality 6 (Fig. 6) and in

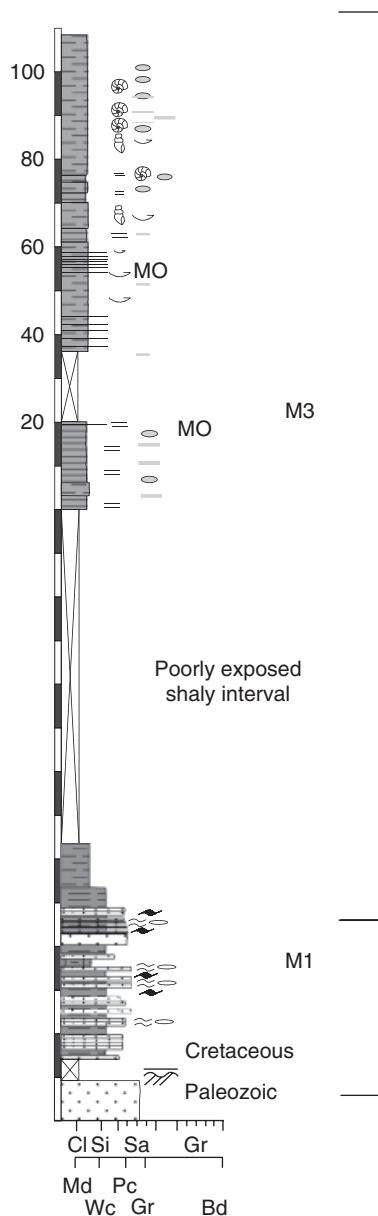


Fig. 10. See location in Fig. 2.

the basal segment at locality 13 (Fig. 10) where it attains 60 m thickness. Sandstones are mostly quartzose. Internally, the beds exhibit flaser, lenticular, wavy, and planar lamination.

The persistent flaser, lenticular and wavy laminations indicate periodic tidal flow in a siliciclastic tidal flat (Reading & Collinson, 1996). These strata are commonly located in the upper part of the described facies associations (e.g. Locality 6, Figs 2 and 6) between transitional to marginal marine environments represented by facies associations B2 and Bt-1, and open-sea shales of facies association M3. Therefore, they reflect an intermediate part in an upward deepening succession.

Facies association M2

Typically, this facies association comprises a cyclic repetition of medium to thin mudstone beds with fine-grained

to very fine-grained sandstones displaying normal grading and erosive to irregular basal contacts. It includes an interval of about 150 m at locality 11 (Fig. 7). These sandstones commonly have tangential cross bedding and tool marks at the base of individual beds. The top of each sandstone cycle is transitional with thin to medium beds of sandy black shales and shales with abundant plant remnants.

The beds with basal erosive contacts, often with tool marks, normal grading, and upper transitional contacts suggest deposition by density currents (e.g. Shanmugam, 1997). A nearby continental source for the turbidites can be inferred from the abundant plant remnants in the interbedded shales. Paleocurrent directions measured on the sole marks (Fig. 7) and a westward pinchout of the sandstones, indicate general flow from continental sources in the east. Turbidites in section 11 probably represent the lateral equivalents of fluvial conglomerates and sandstones in locality 12 to the east.

Facies association M3

This facies consists of monotonous, well-laminated, ammonite-bearing shale beds and rare medium-grained sandstones. Occasionally, the shales contain pyritic laminae or nodules. In some localities there are abundant plant remains interbedded with the shales (e.g. Locality 11). Facies association M3 occurs on top of all other facies associations or represents their lateral equivalent. Because it constitutes a major part of the up to 3-km-thick Berriasian-Valanginian Macanal Formation, its most important feature compared with all other facies associations is its thickness of many hundreds of meters. It is also the only unit with a large lateral extent, covering virtually the entire study area.

Based on the predominant fine-grained lithologies and ubiquitous ammonites, this facies association is interpreted to reflect an open-sea platform environment. The absence of indicators of wave influence or storm beds suggest deposition in the deepest portions of the platform. This is compatible with the pyritic laminae, which is an indicator of anoxic conditions. The presence of plant remains suggests continental proximity.

EARLY CRETACEOUS EXTENSIONAL TECTONICS AND FACIES DISTRIBUTIONS

Our facies analysis demonstrates that the Berriasian depositional settings were spatially highly variable and disparate over short distances, emphasizing the important role of tectonism. Thus, to further understand Berriasian paleogeography, it is necessary to view our analysis in a structural context to evaluate fault controls on local and regional scales. In the following sections, we first describe the main structures in the study area, group them into related segments, and then compare them with the spatial distribution of facies.

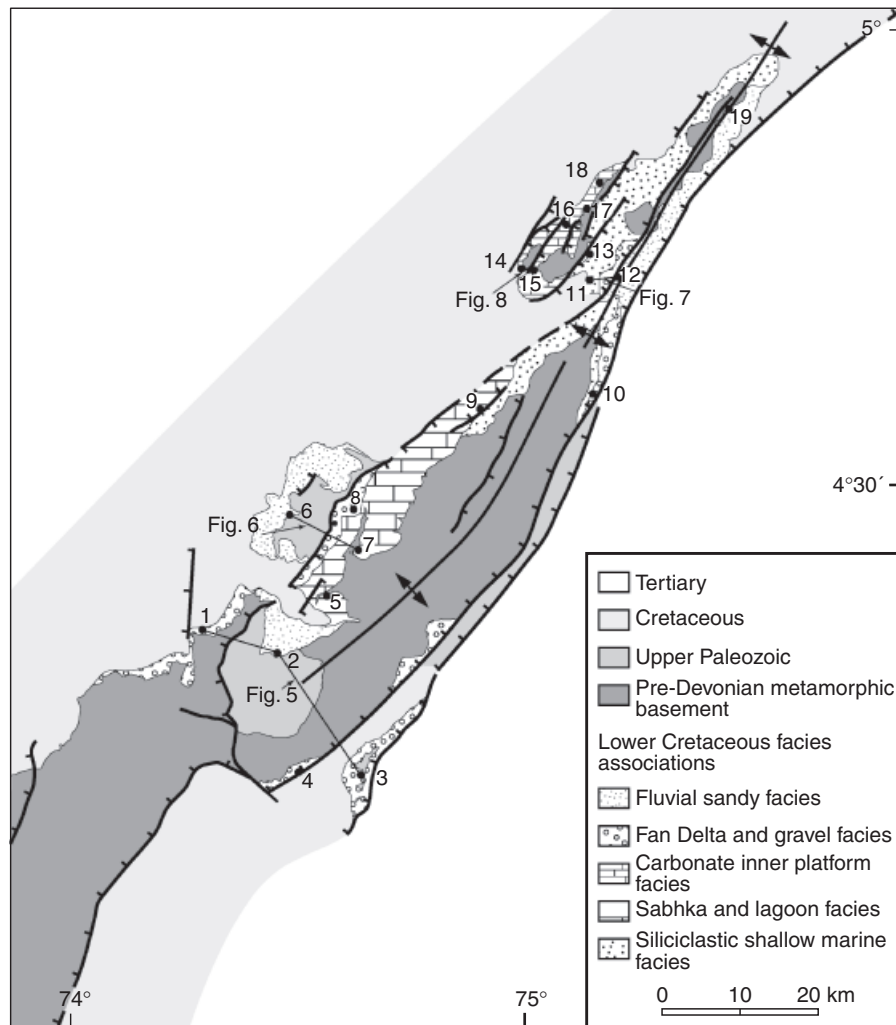


Fig. 11. Map of early syn-rift Cretaceous facies distribution. Notice that the reconstructed distribution of facies does not coincide with the geological map in Fig. 1 as the lateral extent of early syn-rift units has been extrapolated to covered areas. However, post-rift shortening has not been removed, but the normal nature of the faults during the early Cretaceous is shown in the figure.

The structural pattern shows more segmented and pervasive faulting in the northern part of the study area. In contrast, in the south faulting is reduced to less numerous and longer structures. Therefore, we defined two different segments that constitute the Guatiquía paleo-rift. A northern segment comprising the short and rectilinear Gachaluno, Esmeralda, Garabato, Malacara, Miralindo, San Isidro, and Manizales faults (Fig. 2), and a southern segment with the longer Servitá, San Juanito, Naranjal and Los Medios faults (Fig. 2).

Based on the dominant facies association for the first 100 m above the basal unconformity at each location (excluding the ubiquitous lowermost basal conglomerates, if they are thinner than 20 m) and mapping the lateral extension of the facies associations, we compiled a facies map (Figs 2 and 11), in which we depict the earliest stages of Neocomian sedimentation. We also exclude the very local debris-flow deposits in locality 15. We extrapolated the units of interest on the geological map to areas covered by younger strata to the extent admissible from the

mapped contacts. In the facies map it is evident that the lateral extent of many depositional systems appears to be bounded by the traces of the main faults (Fig. 11) as discussed below.

Structural controls on early Cretaceous sedimentation along the different graben segments

In the southern segment shallow marine facies east of the San Juanito fault (facies association C3; localities 5 and 7, Figs 2, 6 and 11) contrast with an up to 300-m-thick basal Cretaceous alluvial sequence west of the same structure (facies association B3; locality 6, Figs 6 and 11). Thus, differential subsidence along this fault presumably controlled these different depositional systems. In addition, the mean grain size of alluvial sequences west of the San Juanito fault decreases southward until they are replaced by shallow marine deposits almost at the southern tip of the San Juanito fault. Therefore, a paleo-high related to

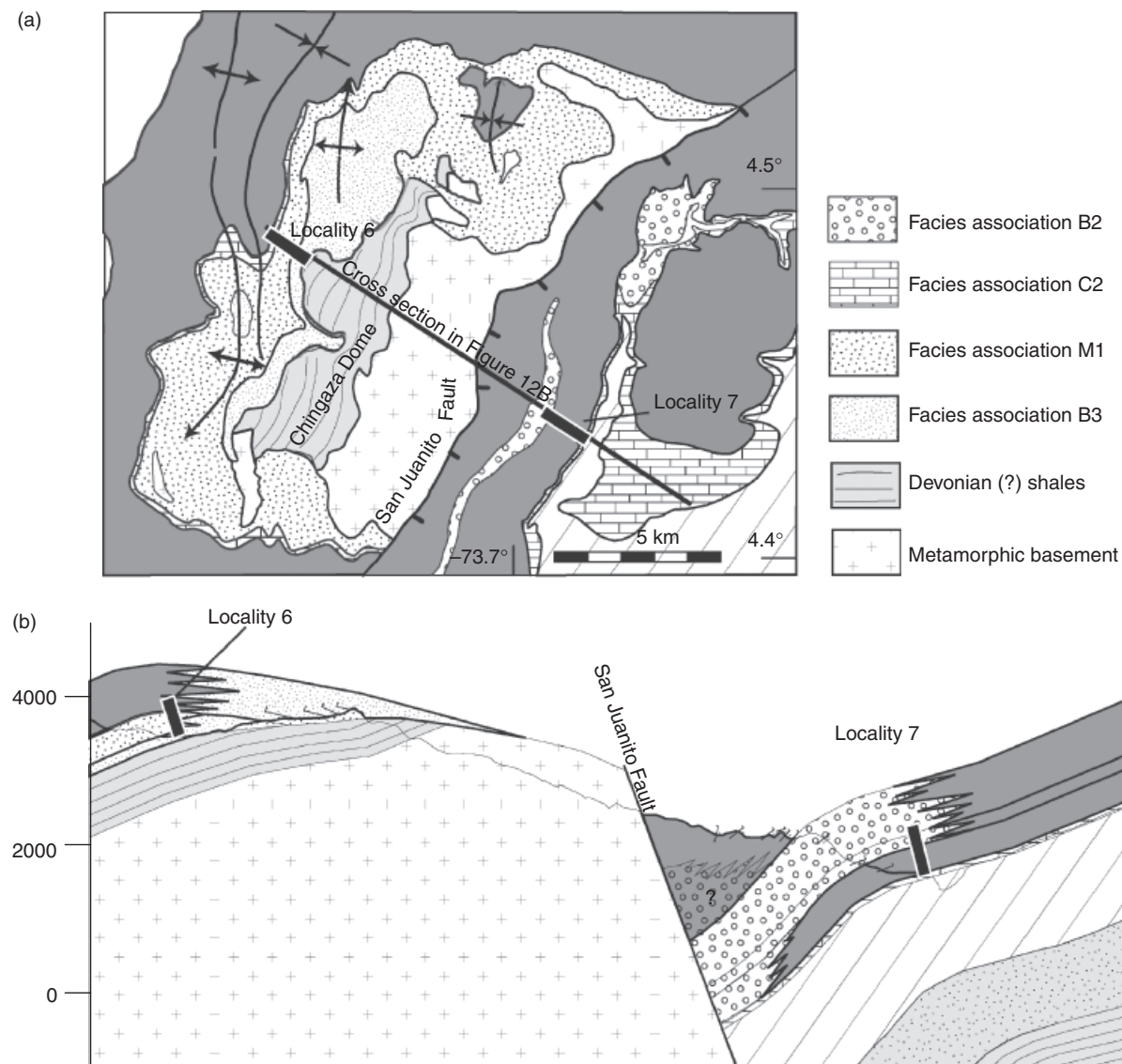


Fig. 12. Detailed geological map and cross section of the Chingaza Dome. Notice that the San Juanito Fault separates a footwall domain to the west where braid and meandering river depositional systems dominate from a domain to the east with fan deltas adjacent to early syn-rift shallow marine systems. See location in Fig. 1.

the San Juanito fault is inferred. We term this paleo-high the Chingaza Dome (Fig. 12). The direction of spatial changes in facies and grain size suggests southward-directed axial drainage west of the San Juanito fault. More significantly, in the southern segment shallow marine facies are restricted to a central area bounded by the Servitá fault to the east and the San Juanito fault to the west (Fig. 11). In this area and all other sectors with marine deposition in the southern segment, laterally restricted fan-delta deposits pinch out (Facies association B2) in a direction perpendicular to all faults in this segment. This pattern can be interpreted as a transverse drainage from the fault-bounded paleo-topographic highs toward the adjacent subsiding areas with marine deposition.

In the northern segment, the Garabato and Malacara faults are associated with an up to 200-m-thick sequence of supratidal evaporites, intertidal stromatolites, and shallow water carbonates (facies associations C1, C2 and C3),

which are restricted to the west of these structures (localities 14, 15, 17 and 18, Figs 8, 11 and 13). In contrast, a 20-m-thick Lower Cretaceous siliciclastic tidal-flat unit above Upper Paleozoic rocks is rapidly superseded up section by distal-platform black shales with ammonites in the eastern block of the Garabato fault (facies associations M1 and M3; Locality 13, Figs 10, 11 and 13). Again, fault controlled differential subsidence can be inferred from these patterns. Shallow-water to supratidal units to the west pinch out near the tips of the Garabato and Miralindo faults, suggesting that these depositional systems also occupied a fault-controlled paleo-high that we term Rio Guavio Dome (Fig. 13). This assessment is corroborated by emerald-bearing mineralizations which are restricted to facies association C2 in the Rio Guavio Dome. These mineralizations have not been reported east of the Garabato and Malacara faults. Other structures like the Manizales and San Isidro faults can be also reinterpreted

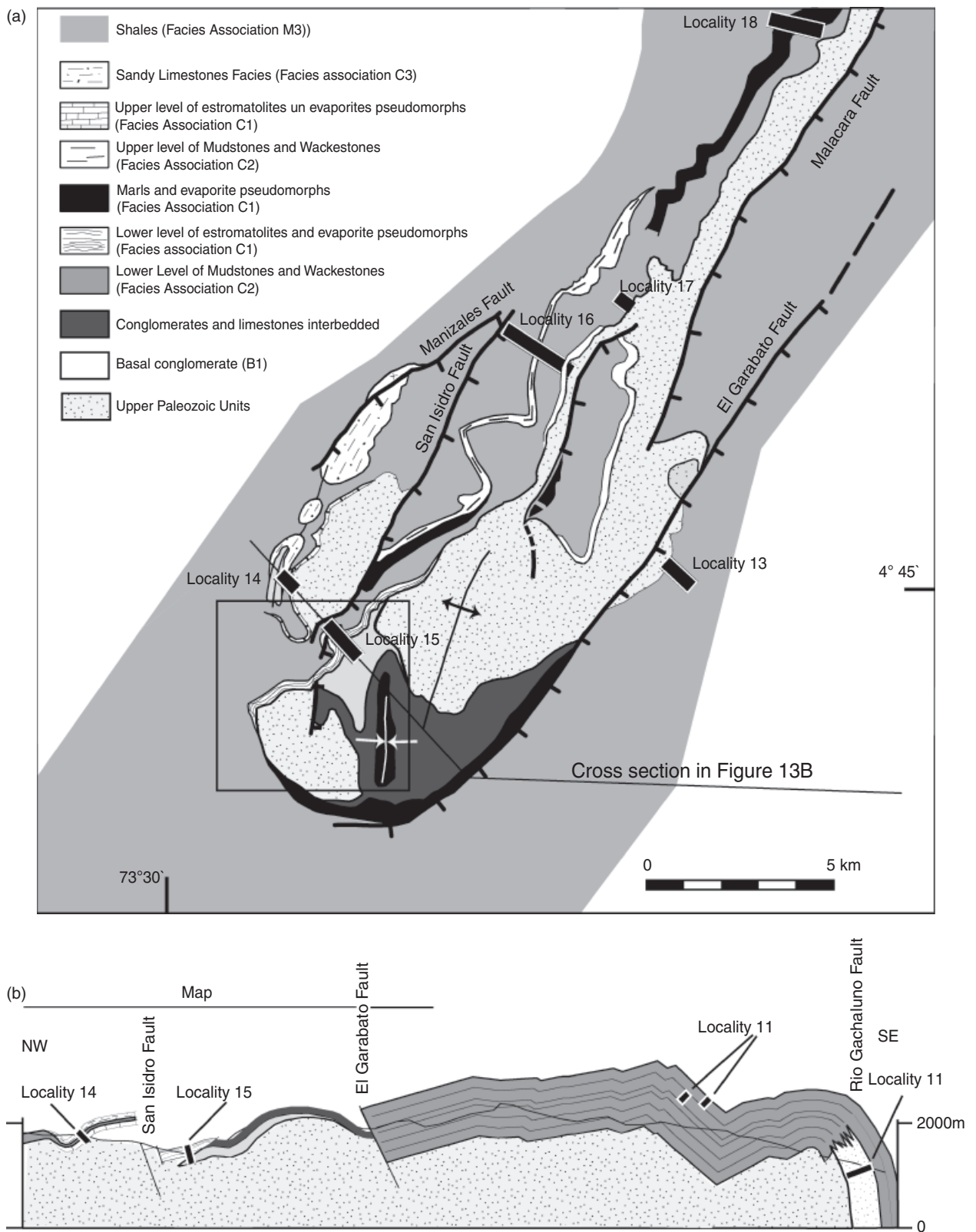


Fig. 13. Detailed geological map and cross section of the Guavio Dome. Notice the map relationships in the area highlighted in the box south of Locality 14; the activity of the normal fault near locality 15 is contemporaneous or even post-dates the deposition of the level of conglomerates and sandstones but pre-dates the deposition of the lower level of stromatolites and evaporite pseudomorphs (Facies association C1). See location in Fig. 1.

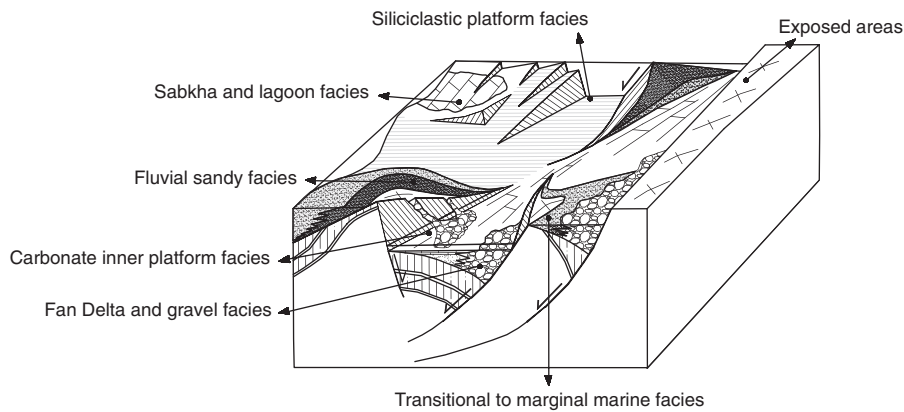


Fig. 14. Idealized configuration of the Lower Cretaceous graben setting (Guatiquía graben) located in the Farallones de Medina region. Not to scale. Notice alluvial units and erosion in the footwalls to the south (southern graben segment) and fan deltas in the hanging wall areas. The supratidal and intertidal units in the footwalls of the northern segment contrast with siliciclastic platform facies in the hanging walls.

as Neocomian faults, because they separate different early syn-rift facies in their hanging and footwalls (Figs 8 and 13). Similarly, the Gachaluno and Esmeralda faults restrict the extent of the sandy-shorezone facies (facies association Bt-1, Fig. 6) of the Bata Formation at localities 11 and 19 (Fig. 11), contrasting with the open-sea shaly facies to the west. In general, faults in the northern segments separate marine facies of different bathymetric affinity. Transverse alluvial to fan-delta depositional systems are only locally present west of the Gachaluno fault.

Taken together, the character and extent of the analyzed facies sequences and structures suggest that virtually all faults in both segments are Neocomian in age. Deposition is therefore interpreted to have been determined by fault activity during the initial phase of rifting. In this extensional scenario, the San Juanito fault in the south was kinematically linked with the Gachaluno fault in the north by an accommodation zone, here called Claraval lineament (Fig. 14). However, the Servitá fault and associated faults to the east are different from all other structures. The rectilinear trace of the Servitá fault contrasts with the discontinuous trace of faults farther west. The Servitá fault system along the eastern boundary of the study area also constitutes the depositional boundary of Neocomian strata to the east. We therefore differentiate the Servitá fault as a basin-boundary fault contrasting with the intrabasinal faults to the west. In the northern graben segment an equivalent principal Neocomian boundary fault is not discernible from field data, although it should be located along strike of the Servitá fault, as can be inferred from seismic and gravimetry data (e.g. Mora *et al.*, 2006).

West of the Servitá fault, irrespective of the structural position, and therefore along all of the intrabasinal structures of the northern and southern segments, there is evidence for a ubiquitous rapid vertical transition from shallow marine and fluvial facies to more distal marine to deep marine shaly facies. In addition, Berriasian to Valanginian black shales often attain more than 2 km thickness (e.g. locality 17) whereas underlying alluvial and shallow

marine sequences are rarely thicker than 500 m. Total accommodation space may apparently have increased after the deposition of shallow-marine and alluvial sequences as intrabasinal footwall blocks were covered by marine sediments, either due to decreased activity or locking of faults. In contrast, pre-Aptian rocks are absent east of the Servitá fault and associated basin boundary structures (e.g. Figs 16 and 17). Therefore, these faults continued to be active until the Aptian. Figure 13 (see normal fault south of locality 15), 17 and 18 show structural relationships documenting some cases where the intrabasinal faults to the west of the basin bounding faults were active only during short periods, as mapped Berriasian horizons clearly post-date the faults.

Footwall uplift patterns

Structural mapping reveals that in the southern segment of the Guatiquía paleo-rift paleozoic rocks are absent directly to the east of the Servitá fault (Figs 1 and 11, Locality 3). However, at locality 10 west of the Servitá fault, a Berriasian debris-flow deposit pinches out to the west and evolves into sandy turbiditic facies (Fig. 17), indicating a higher source area to the east. The provenance of these debris-flow deposits identifies a source region in Paleozoic sedimentary rocks (Table 1 see Locality 10). Phyllite clasts do not occur, although the faulted contact of the debris-flow deposits to the east is against phyllites of the Quetame Group (Fig. 17). The structural and stratigraphic relationships at locality 10 (Fig. 17) thus show that Paleozoic rocks were present east of the Servitá fault but eroded before, and during the onset of Cretaceous deposition. Erosion of Paleozoic rocks before, and during the onset of Cretaceous deposition is also documented in the western block of the San Juanito fault by map patterns (Fig. 12; Mora *et al.*, 2006) and sandstone petrography from Parra (2000). Interestingly, except localities 1 and 10, all sites in the southern segment of the graben contain numerous clasts of phyllites coming from the Quetame Group (see

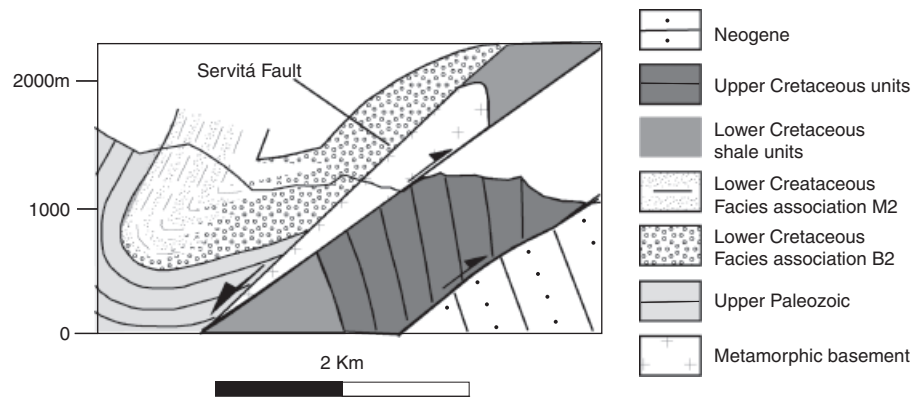


Fig. 15. Detailed cross section along the Arditá Creek. Notice the westward granulometric change in the Early Cretaceous facies to the west and the presence of a block without Paleozoic cover below the Early Cretaceous units. See 'Discussion' in the text.

Table 1 and Fig. 11). This observation, and the presence of debris-flow units adjacent to the fault-bounded paleo-topographic highs, document that there was footwall uplift along the faults bounding the southern graben. This uplift must have been pronounced, creating high terrain from which basement clasts were eroded and transported to the hanging-wall basins. These processes were ultimately responsible for the removal of *ca.* 3 km of upper Paleozoic rocks before the onset of Cretaceous deposition on these structural highs (see generalized configuration in lower part of Fig. 14).

In contrast, in the northern segment and north of locality 10 there are no surface exposures of the Quetame Group phyllites and quartzites immediately below the Cretaceous section (Fig. 11). Underlying units belong to upper Paleozoic sedimentary strata. Interestingly, metamorphic clasts are absent in the basal conglomerates in sections 10–19 in the northern segment (Table 1). In addition, local debris-flow sequences were only observed in the hanging-walls of the San Isidro and Gachaluno faults (Figs 7 and 8). Therefore, the provenance and areal extent of sediments document that footwall uplift was either negligible or absent in the northern segment (compare lower and upper part of Fig. 14).

Footwall-uplift patterns are observed along faults dipping both west and east (Figs 2, 14 and 16) in both segments. Therefore, we hypothesize that the eastern faults with the footwall to the east, were active at the same time and probably interacted mechanically with the corresponding western faults and their footwalls. However, it is not clear whether the southern and northern graben segments were active coevally. Since the work of Jackson & McKenzie (1983), footwall uplift in many extensional provinces has been documented to be proportional to adjacent hanging-wall subsidence. If that is also true for our study area, hanging-wall subsidence in the southern segment should have been higher than in the north. Accordingly, we do not interpret the early deposition of marine sequences in the footwall blocks of the northern segment to reflect an increase in total tectonic subsidence with respect to the southern segment, but rather reduced local footwall uplift.

STYLES OF REACTIVATION

Superimposed Cenozoic contraction along the extensional structures generated many significant structural features in the Eastern Cordillera. At all scales, former extensional basement highs appear to have confined contractional folding structures (Fig. 15). A clear example is the Rio Los Medios syncline, where the former extensional hanging wall of the Los Medios normal fault has been folded in contraction against the former extensional footwall uplift (Fig. 18). This behavior, defined as basement buttressing, has been identified as a typical form of reactivation by Mora *et al.* (2006) in the Eastern Cordillera. The most representative large-scale examples of basement buttressing are the Farallones and Santa María anticlines (Figs 2 and 15). All of the documented Neocomian faults confine the areal extent of both structures (Figs 2, 13 and 15). The Farallones anticline coincides with the hanging-wall sectors in front of the normal faults at the southern segment of the Guatiquía graben, whereas the Santa María anticline coincides with downthrown areas in the northern segment, clearly identifying them as inversion anticlines. In contraction, the Claraval lineament also forms a transfer zone as the Farallones and Santa María anticlines are distributed in en-echelon manner along this structure. Therefore, there is a fundamental basement-related predisposition of faulting and folding in this part of the northern Andes. This has resulted in differences in inversion-generated structural relief and reactivation along pre-existent fault planes, which we will discuss for the southern and northern segments. We illustrate these differences by comparing paleo-topography deduced from the facies map (Fig. 11) with present-day topography (Fig. 2), and by employing serial balanced cross-sections (Fig. 15).

Reactivation in the southern graben segment

In the southern graben segment, the basal Cretaceous unconformity in the hinge zone of the Farallones anticline lies at *ca.* 4000 m above sea level, the maximum elevation of this horizon in the study area (Figs 2 and 15). The location of the Farallones anticline coincides with the zone of

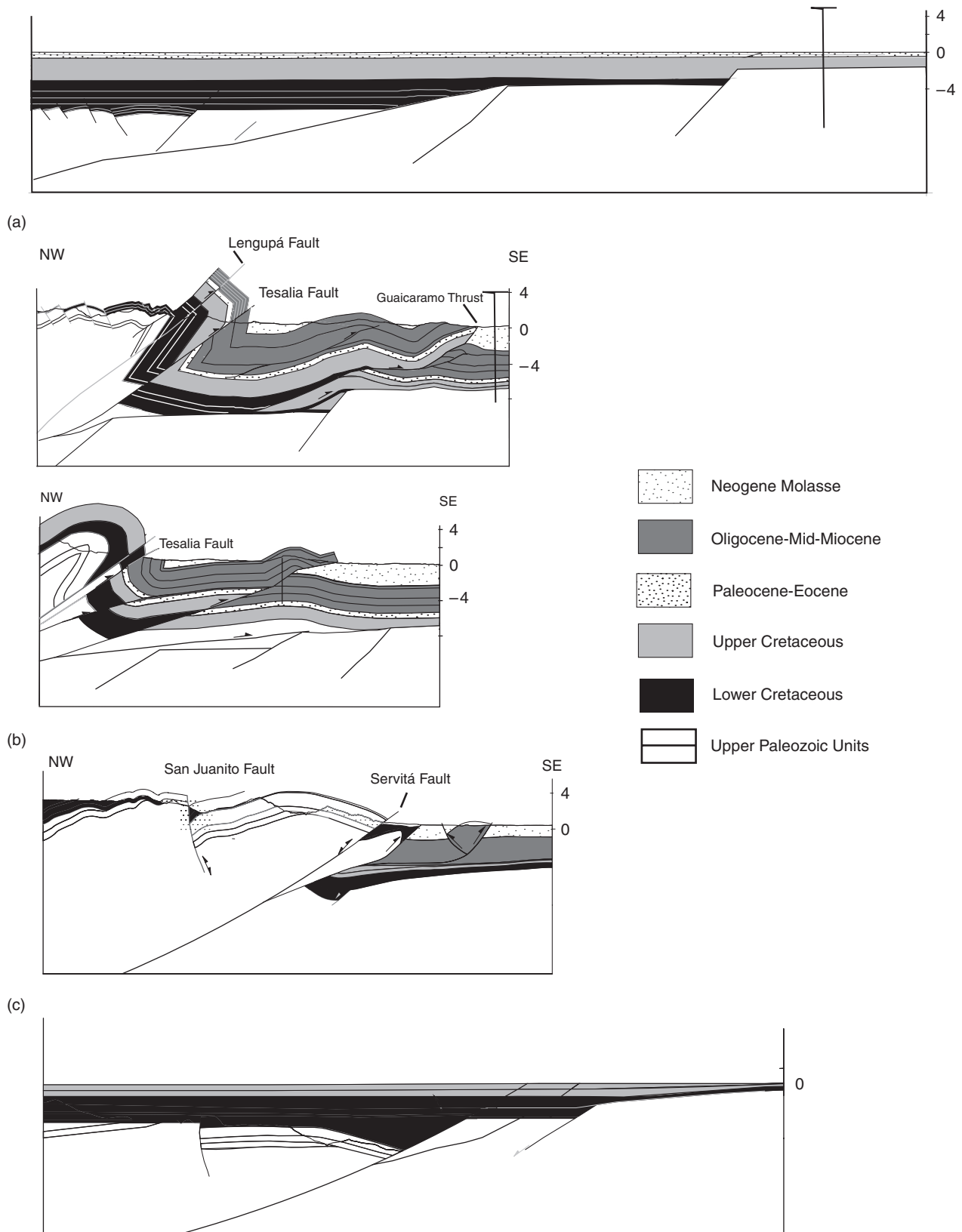


Fig. 16. Balanced cross sections along the different segments of the study area. (a) Cross section along the northern segment. Note that the present day active foreland deformation front is also included. Below a retrodeformed Eocene state is included. (b) Cross-section along the central segment of the study area. (c) Cross section along the southern segment of the study area, in the lower part a Maastrichtian-Paleocene retrodeformed state is included. Notice how fault propagation folding is minor along the Servitá fault compared with prominent fault propagation folding in the central and northern cross-sections associated with the Tesalia and Lengupá thrusts. In contrast, shortening in the central and northern cross-sections is absorbed mostly by the Guaicáramo Thrust. See locations in Fig. 1.

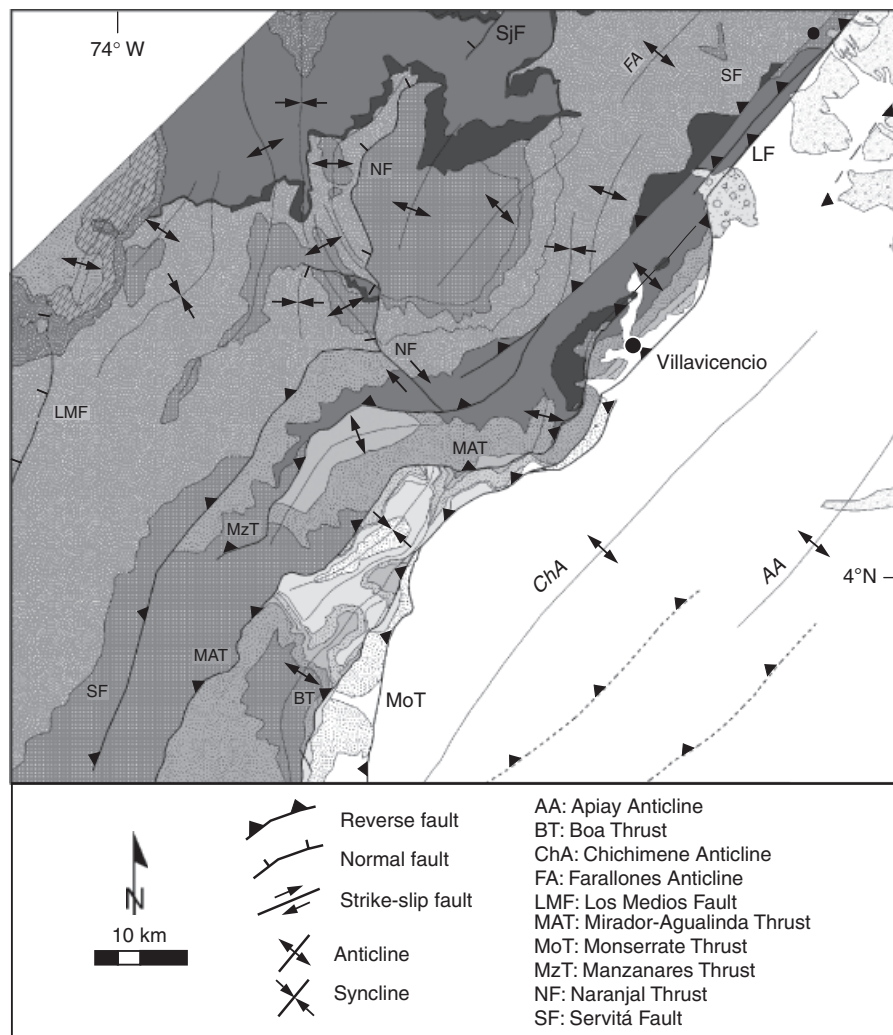


Fig. 17. Geological map of the southernmost part of the study area. Symbols are the same as in Fig. 1. The Lower Cretaceous Servitá basin bounding fault can be identified as the structure that bounds the area where Upper Paleozoic sequences are preserved above the pre-Devonian metamorphic basement (Quetame Group). In contrast, east of this structure Lower Cretaceous rocks rest on top of pre-Devonian metamorphic basement. Therefore structures east of the Servitá fault can be interpreted as footwall shortcuts. Symbols are the same as in Fig. 1. See location in Fig. 1.

maximum extensional subsidence during the Cretaceous. Despite this, many paleo-topographic highs in extension have retained their character as topographic highs during contraction. For example, the alluvial facies in the footwall of the San Juanito fault (locality 6) or the southernmost exposures of syn-rift rocks in the Farallones anticline (locality 2) coincide with structural and topographic culminations at elevations near 4000 m above sea level (compare Figs 2 and 11). We therefore posit that maximum inversion-generated structural relief appears to coincide with zones of maximum extensional subsidence, although adjacent paleo-topographic highs have remained as topographic highs in contraction.

The contractional reactivation (displacement) in the southern segment along the faults themselves appears to be concentrated along the reactivated basin-boundary faults and associated shortcuts (Figs 2 and 11). For example, it is evident that reverse displacement along the Servitá fault during contraction is generally limited. However,

the Servitá fault was only reactivated in contraction at its southern termination and remained in net extension near its northern termination (Fig. 15). In addition, most of the contractional fault displacement and shortening on the eastern flank of the Eastern Cordillera is due to the Mirador shortcut thrust (Fig. 1). This shortcut branches from the Servitá fault, an interpretation supported by seismic profiles and the fact that in map view this structure is always parallel to the Servitá fault, except near its tips which converge with the trace of the Servitá fault (Figs 1 and 15). Therefore, these map patterns may represent an oblique view of converging thrusts at depth, as has been observed in many thrust systems (e.g., Boyer and Elliot, 1982). The Servitá fault and Mirador shortcut account for *ca.* 20 km of shortening in the Eastern Cordillera as deduced from line-length balanced cross-sections (Fig. 15). In contrast, intra-basinal faults with their footwalls to the west, such as the San Juanito Fault, only accommodated minor reactivation (Mora *et al.*, 2006, Fig. 15). It therefore appears that

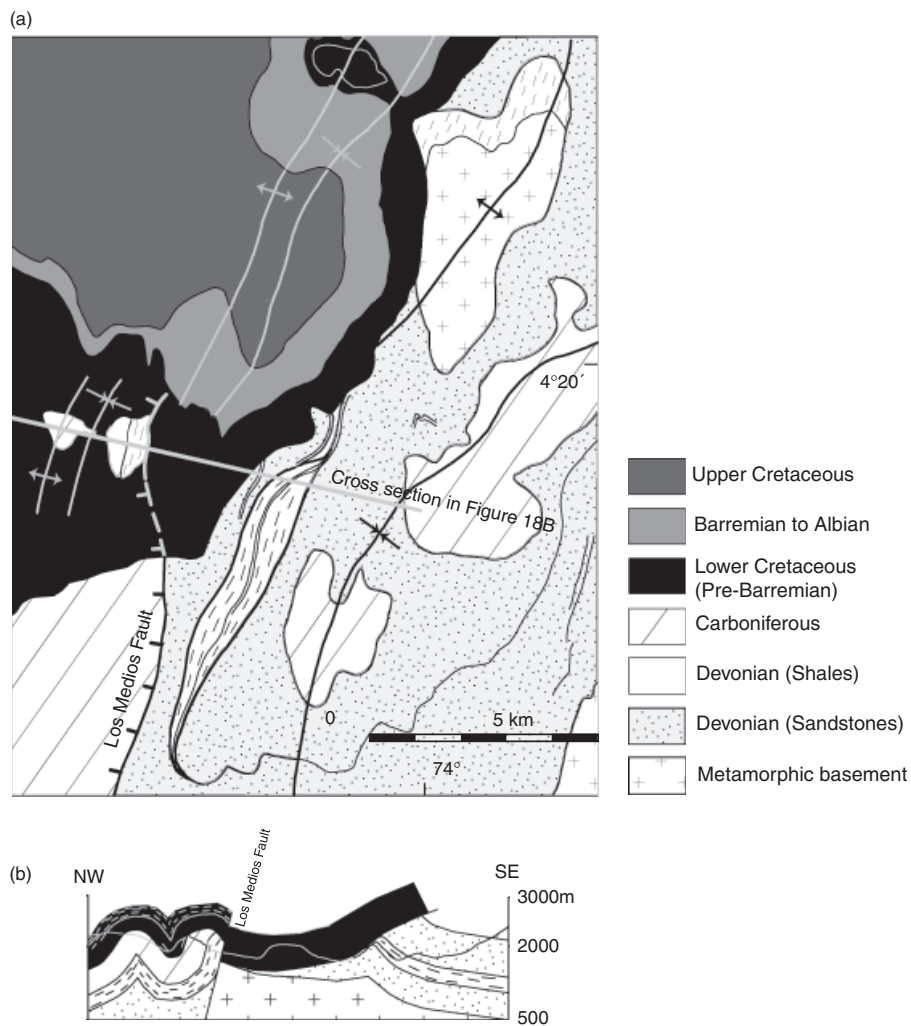


Fig. 18. (a) Detailed geological map of the Los Medios fault. Notice the map expression of pronounced footwall uplift before the onset of deposition of Lower Cretaceous strata. On the other hand Barremian units post-date the activity of the Los Medios fault. (b) Reactivation along the plane of the Los Medios fault has been limited but tight folding west of Los Medios fault attests for the Los Medios footwall acting as a stress riser buttressing the folds to the west.

the intrabasinal Neocomian highs like San Juanito footwall remained in high topographic positions, mainly because they were passively transported by the Servitá fault.

Reactivation in the northern graben segment

As in the south, in the former northern graben segment, maximum inversion-generated structural relief coincides with areas of maximum Neocomian subsidence, such as the hinge zone of the Santa Maria anticline (Fig. 2). Accordingly, paleo-highs in the northern segment, (e.g. the Rio Guavio paleo-high) have retained their character as structural culminations in contraction with respect to the elevation of the basal Cretaceous unconformity. However, with elevations of about 2200 m, structural culminations in the north lie at substantially lower elevations than in the south.

Maximum fault displacement in the northern segment is concentrated along structures that lie along strike north of the Servitá fault, including the Lengupá and Tesalia faults. Neither one of these structures have been unequivocally

documented as a Lower Cretaceous structures. There is also no evidence that they constitute shortcuts branching out from inherited structures, and the amount of slip is minor compared with equivalent reactivated faults along strike in the southern segment (e.g., Servitá fault, Fig. 15). Adjacent normal faults like the Gachaluno fault have not been reactivated in contraction (Fig. 2). In contrast, it is striking that a vertical to overturned panel of Tertiary and Cretaceous rocks, associated with the Lengupá and Tesalia faults, bounds the entire Santa Maria anticline to the east. No comparable panel exists in the southern segment (Figs 2 and 15). Therefore, most of the basin inversion in the northern segment is due to fault-propagation folding, rather than direct displacement along reactivated faults or footwall shortcuts. Furthermore, shortening accumulated by faulting and fault-propagation folding in the forelimb of the Santa Maria anticline is close to 20 km, similar to the ca. 20 km of shortening to the south in that case almost only due to faulting (Fig. 15).

Interestingly, if the displacement trends of the paleotopographic highs like the Rio Guavio and Chingaza domes

are compared along strike, a displacement deficit results in the area between both, in extension as well as in contraction. This is probably related with displacement transfer towards basin bounding structures through the Claraval accommodation zone, both in extension and in contraction. Conversely, reactivated faults bounding the Farallones and Santa Maria anticlines to the east show what Walsh *et al.* (2003) called a sympathetic increase and decrease in displacement, without displacement gaps.

DISCUSSION AND CONCLUSIONS

Careful mapping and analysis of Neocomian facies associations coupled with structural investigations suggest that faults in the Farallones anticline domain originated as extensional faults during the early Cretaceous. Facies and provenance analysis enable us to distinguish former southern and northern rift segments that formed an integral part of the Guatiquía paleo-rift. In the southern segment, during early syn-rift deposition (Facies associations C and B), tectonic subsidence was higher compared with the northern segment. Early syn-rift deposition in the southern segment was associated with adjacent areas of high paleo-topography in footwall areas (Fig. 14). This is true for both intrabasinal and basin boundary faults in this segment where shallow marine facies and fan deltas characterize subsiding areas, while alluvial facies were deposited in paleo-highs. In contrast, north of about 4°30'N a more segmented northern rift sector existed during rift initiation (Facies associations C, B, Bt). Here, as deduced from footwall uplift, intrabasinal and basin-boundary faults accrued less displacement than structures in the southern segment. Shallow marine facies dominate in hanging-wall areas, whereas sabkha facies characterize footwall sectors. Intrabasinal faults in both the southern and northern segments account for a highly variable early syn-rift facies distribution due to isolated depocenters and paleo-highs. This is exemplified by the Chingaza and Rio Guavio domes, which restrict the areal extent of Cretaceous depositional systems. Segmented faults, isolated depocenters, and paleo-highs during rift initiation show that intrabasinal fault systems evolved from localized areas of extension and grew along strike through segment linkage (e.g. Cartwright *et al.*, 1995; Dawers & Anders, 1995). In the northern part of the rift, individual faults are more numerous, shorter and rectilinear, reflecting less advanced fault linkage (e.g. Gawthorpe & Leeder, 2000). Accordingly, a more internally structured northern rift, coupled with the spatial patterns of footwall uplift, may have resulted from either rift propagation from south to north or northward extensional displacement gradients (Cowie *et al.*, 2000) (Fig. 2). From the relationships between faulting and sedimentation observed here, we propose that east-dipping intra-basinal faults (e.g., San Juanito and Garabato faults) interacted mechanically with faults farther east (e.g. Servitá fault) during rift initiation.

Subsequently, the rapid overall facies transition from 'rift initiation' (*sensu* Prösser, 1993. Facies associations B, C and Bt) to the fine grained 'rift climax' sedimentation (*sensu* Prösser, 1993. Facies associations M) marks the onset of an episode where subsidence was rapid adjacent to the Servitá fault. Footwall uplift along this structure was protracted, contrasting with intrabasinal faults whose footwall areas were already submerged. Thus, footwall uplift of the intrabasinal faults was subdued compared with basin subsidence associated with the eastern boundary faults. This, and the widespread complete Cretaceous sequence west of the major boundary faults demonstrate that intrabasinal faults remained inactive until their Cenozoic inversion. In contrast, the onset of Cretaceous deposition east of the Servitá fault only occurred during the Albian. Thus, total syn-rift displacement along the basin-boundary faults appears to have been greater than along the intrabasinal faults. If true, the early linkage of the intrabasinal faults was interrupted during the rift climax. Therefore, the fault pattern that we observe in the intrabasinal faults represents the pattern of growth during the rift initiation stage.

In this context, it is worth noting that in the southern segment the Servitá fault is rectilinear and displays no evidence for earlier coalescing segments that would suggest growth through linkage (Trudgill & Cartwright, 1994; Cartwright *et al.*, 1995; Dawers & Anders, 1995). Therefore, we propose that the facies transition from 'rift initiation' to 'rift climax' is not related to enhanced subsidence after linkage (Gupta *et al.*, 1999; Cowie *et al.*, 2000), but rather to an increased displacement along the principal basin-boundary faults. The overall structural evolution suggests that the intrabasinal Neocomian faults may represent antithetic collapse structures associated with a major roll-over anticline in the hanging-wall of the eastern boundary faults, analogous to the central Kenya Rift (Roessner & Strecker, 1997), the Viking Graben (Roberts & Yielding, 1991) or the collapse grabens in analog models of listric faults (Mitra, 1993; McClay, 1995; Withjack *et al.*, 1995; Yamada & McClay, 2004; Seyferth & Henk, 2006).

Cenozoic shortening in the Eastern Cordillera of Colombia is fundamentally influenced by the inherited extensional structures. During contraction, the principal bounding faults experienced a higher degree of reactivation, with throw reversing the extensional offset (Fig. 15). There is more efficient reactivation along the Servitá fault/Mirador shortcut pair in the southern segment compared with the northern Lengupá and Tesalia faults. In the northern segment, fold propagation dominates over direct slip. Interestingly, footwall uplift was absent or negligible during the Neocomian in the northern segment, whereas in the southern segment footwall topography was pronounced. Thus, if footwall uplift is a proxy for extensional subsidence in the adjacent hanging wall (Jackson & McKenzie, 1983), areas undergoing maximum extensional displacement also tend to focus reverse displacement along former border faults (Fig. 15). Accordingly, zones of maximum Cenozoic inversion-generated uplift (i.e. reverse fault displacement plus anticlinal fold amplitude)

appear to coincide with zones of maximum Neocomian extensional displacement and subsidence, like the Faralones anticline in the southern segment. These observations are similar to those of Underhill & Paterson (1998) in the Wessex basin. In addition, we also find similarities with 3D analog inversion models (Yamada & McClay, 2004), suggesting inheritance of along-strike displacement gradients in the extensional province.

In contrast to the major basin bounding faults, reactivation of the much more segmented intrabasinal faults was less pronounced. As a consequence, syn-extensional paleo-topographic highs were passively uplifted and persisted as topographically elevated areas in contraction, with similar segmentation and displacement gaps. It is likely that focused faulting along rectilinear basin-bounding structures in both extension and in contraction identifies these structures as long-lived, predisposed zones of weakness in the crust, similar to observations in the Gamtoos basin (Paton & Underhill, 2004) of South Africa. In such a scenario, fault length in extension is defined early during rifting (Walsh *et al.*, 2002). If fault segments exist, they define a kinematically coherent system that merges into a single structure at depth (Walsh *et al.*, 2003), contrasting with growth through linkage. Interestingly, in the foreland east of the basin-boundary faults, upper Paleozoic rocks were not encountered in exploratory wells, and Andean phyllitic basement rocks are replaced by Guyana shield basement (e.g. Dueñas, 2002). In addition, the existence of the basin-bounding faults as pre-Mesozoic multi-phased structures is supported by many studies (e.g. Forero-Suarez, 1990). This could provide a mechanism for the initial rapid Mesozoic trace lengthening and subsequent preferential fault reactivation. In this context, it is clear why intrabasinal faults that grew through linkage are subordinate anisotropies compared with the longer basin-bounding structures.

These observations raise the question as to which factor defined the observed growth mechanisms for the intrabasinal structures. Walsh *et al.* (2003) argue that an incidental linkage of otherwise isolated faults is more likely where a pre-existent coherent weakness is absent and faulting has to randomly break through a mechanically heterogeneous multilayer. Interestingly, in contraction we document either direct reactivation or shortcuts branching from the basin margin faults while intrabasinal faults remained undisturbed. We interpret this pattern to indicate that, irrespective of long-lived basement fabrics, segmented extensional structures that purely grew through linkage of individual faults may be less prone to inversion than normal faults that propagated upward from a coherent common plane.

In summary, our paleogeographic reconstruction of the early syn-rift setting in the northern Andes provides a unique comparison between extensional tectonics and subsequent orogenic contraction. As in other inversion provinces (e.g. Coward *et al.*, 1989; Graciansky *et al.*, 1989; Bailey *et al.*, 2002; Kley *et al.*, 2005; Carrera *et al.*, 2006), the fundamental imprint of pre-existent basement fabrics has generated direct reactivation, with buttresses and shortcuts as typical in-

version features. However, our observations show that inheritance of lateral displacement gradients and the mechanism of extensional fault growth itself are additional, important factors also influencing inversion styles in contractional orogens. These phenomena may be more common than previously thought. Importantly, only those extensional structures which coincide with basement features that existed before the extensional phase profoundly determine the width of the contractional orogen. In addition selective fault reactivation in contraction appears to be related to the style of extensional fault growth, and not only to the orientation of the compressional stresses with respect to the pre-existent normal faults as previously proposed in this region (e.g. Mora *et al.*, 2006).

Our observations are useful in the extrapolation of features observed in analog models and mild to moderately inverted intra-plate basins to the structures of inverted orogens. In the latter case, shortening is often more intense and the relationships between ancestral extensional segmentation and superimposed past or ongoing contraction are less clear. However, geometries and patterns of inversion in orogens and intra-plate areas are comparable. Our analysis helps understand and predict the behavior of many structural and stratigraphic traps of extensional origin incorporated in contractional settings. The documented features are therefore important for fossil fuels or mineral deposits exploration, particularly in frontier intra-plate or orogenic areas that normally rely on limited subsurface data sets.

ACKNOWLEDGEMENTS

The authors are indebted to Arndt Peterhansel, Estelle Mortimer, Gabriela Marcano, Cornelius Uba and Jessica Zamagni for interesting discussions that improved the ideas in this paper. Cornelius Uba and Jessica Zamagni graciously read an earlier version of this paper.

Careful reviews by Nestor Cardozo, William Cavazza and Brian Horton improved the final version of this manuscript. Funding for field work came from Leibniz funds to M. Strecker (DFG STR373/16-1) and the Geological Survey of Colombia (Ingeominas, project Cinturones Esmeraldíferos de la Cordillera Oriental). A. Mora and M. Parra are grateful to the DAAD for funding their stay at the Geosciences Department at the University of Potsdam. Birgit Fabian made Figs 2 and 11. Dr Fernando Etayo-Serna (Ingeominas) determined the relative ages of the ammonites available in our profile locations. Oscar Fernandez from Midland Valley provided a 2dMove license for balancing our cross sections. Sara Morón and Jaime Corredor assisted our work in the field.

REFERENCES

- ALSHARHAN, A.S. & KENDALL, C.G.St.C. (2003) Holocene coastal carbonates and evaporites of the southern Arabian Gulf and their ancient analogues. *Earth Science Rev.*, **61**, 191–243.

- BADLEY, M.E. (2001) Late tertiary faulting, footwall uplift and topography in Western Ireland. In: *The Petroleum Exploration of Ireland's Offshore Basins* (Ed. by P.M. Shannon, P.D.W. Haughton & D.V. Corcoran, *Geol. Soc. Spec. Publ.*, **188**, 201–207.
- BAILEY, C.M., GIORGIS, S. & COINER, L. (2002) Tectonic inversion and basement buttressing: an example from the central Appalachian Blue Ridge Province. *J. Struct. Geol.*, **24**, 277–304.
- BEAUCHAMP, W., ALLMENDINGER, R.W., BARAZANGI, M., DEMNATI, A., EL ALJI, M. & DAHMANI, M. (1999) Inversion tectonics and the evolution of the High Atlas Mountains, Morocco, based on a geological-geophysical transect. *Tectonics*, **18**, 163–184.
- BLAIR, C.T. & MCPHERSON, J.G. (1998) Recent debris-flow processes and resultant form and facies of the dolomite alluvial fan, Owens Valley, California. *J. Sediment. Res.*, **68**, 800–818.
- BOYER, S.E. & ELLIOT, D. (1982) Thrust systems. *AAPG Bulletin*, **66**, 1196–1230.
- BÜRGL, H. (1961) El Jurásico e Infracretáceo del Río Batá, Boyacá. *Bol. Geol. Inst. Geol. Nac.*, **6**, 169–211.
- CARRERA, N., MUÑOZ, J.A., SÀBAT, F., MON, R. & ROCA, E. (2006) The role of inversion tectonics in the structure of the Cordillera Oriental (NW Argentinean Andes). *J. Struct. Geol.*, **18**, 1921–1932.
- CARTWRIGHT, J.A. (1989) The kinematics of inversion in the Danish Central Graben. In: *Inversion Tectonics* (Ed. by M.A. Cooper & G.D. Williams), *Geol. Soc. Spec. Publ.*, **44**, 153–175.
- CARTWRIGHT, J.A., TRUDGILL, B.D. & MANSFIELD, C.S. (1995) Fault growth by segment linkage: an explanation for scatter in maximum displacement and trace length data from the Canyonlands grabens of SE Utah. *J. Struct. Geol.*, **17**, 1319–1326.
- CHAPMAN, T.J. (1989) The Permian to Cretaceous structural evolution of the Western Approaches Basin (Melville sub-basin), UK. In: *Inversion Tectonics* (Ed. by M.A. Cooper & G.D. Williams), *Geol. Soc. Spec. Publ.*, **44**, 177–200.
- COLLETTA, B., HEBRARD, F., LETOUZEY, J., WERNER, P. & RUDKIWEICZ, J.L. (1990) Tectonic style and crustal structure of the Eastern Cordillera, Colombia from a balanced cross section. In: *Petroleum and Tectonics in Mobile Belts* (Ed. by J. Letouzey), pp. 81–100. Editions Technip, Paris.
- COLLINSON, J.D. (1996) Alluvial sediments. In: *Sedimentary Environments: Processes, Facies and Stratigraphy* (Ed. by H.G. Reading), pp. 37–82. Blackwell Science, Oxford.
- COWARD, M.P., ENFIELD, M.A. & FISCHER, M.W. (1989) Devonian basins of Northern Scotland: extension and inversion related to Late Caledonian-Variscan tectonics. In: *Inversion Tectonics* (Ed. by M.A. Cooper & G.D. Williams), *Geol. Soc. Spec. Publ.*, **44**, 275–308.
- COWIE, P.A., GUPTA, S. & DAWERS, N.H. (2000) Implications of fault array evolution for synrift depocentre development: insights from a numerical fault growth model. *Basin Res.*, **12**, 241–261.
- DALRYMPLE, R.W. & CHOI, K. (2007) Morphologic and facies trends through the fluvial-marine transition in tide-dominated depositional systems: a schematic framework for environmental and sequence-stratigraphic interpretation. *Earth Sci. Rev.*, **81**, 135–174.
- DAVIS, D., SUPPE, J. & DAHLEN, F.A. (1983) Mechanics of fold-and-thrust belts and accretionary wedges. *J. Geophys. Res.*, **88**, 1153–1172.
- DAWERS, N.H. & ANDERS, M.H. (1995) Displacement-length scaling and fault linkage. *J. Struct. Geol.*, **17**, 607–614.
- DORADO, J. (1992) Contribución al conocimiento de la Estratigrafía de la formación Brechas de Buenavista (límite Jurásico-Cretácico), región noroeste de Villavicencio (Meta). *Geol. Colombiana*, **17**, 7–40.
- DUEÑAS, H. (2002) Paleozoic palynological assemblages from the Colombian Llanos Basin. *34th. Annual Meeting of the American Association of Stratigraphic Palynologists*, 2001, San Antonio, Texas. *Palynology*, **26**, p. 264.
- EISENSTADT, G. & WITHJACK, M.O. (1995) Estimating inversion: results from clay models. In: *Basin Inversion* (Ed. by J.G. Buchanan & P.G. Buchanan), *Geol. Soc. Spec. Publ.*, **88**, 119–136.
- ETAYO-SERNA, F., SOLÉ-DE PORTA, N.S., DE PORTA, J. & GAONA, T. (2003) The Batá formation of Colombia is truly Cretaceous, not Jurassic. *J. South Am. Earth Sci.*, **16**, 113–117.
- FORERO-SUAREZ, A. (1990) The basement of the Eastern Cordillera, Colombia: an allochthonous terrane in northwestern South America. *J. South Am. Earth Sci.*, **3**, 141–151.
- FÜRSICH, F.T. (1995) Shell concentrations. *Eclogae Geol. Helv.*, **88**, 643–655.
- GALLOWAY, W.E. & HOBDAV, D.K. (1996) *Terrigenous Clastic Depositional Systems: Applications to Fossil Fuel and Groundwater Resources*, 2nd edn. Springer, Berlin.
- GARCÍA SENZ, J. (2002) Cuencas extensivas del Cretácico Inferior en los Pirineos centrales: formación y subsecuente inversión. PhD Thesis, Universitat de Barcelona, Barcelona.
- GAWTHORPE, R.L. & LEEDER, M.R. (2000) Tectono-sedimentary evolution of active extensional basins. *Basin Res.*, **12**, 195–218.
- GEMMER, L., NIELSEN, S.B. & BAYER, U. (2003) Late Cretaceous-Cenozoic evolution of the North German basin: results from 3-D geodynamic modelling. *Tectonophysics*, **373**, 39–54.
- GEOSTRATOS (2005) Columna estratigráfica Río Chivor, Ingeominas. Bogotá, Colombia. Internal Report, 21p.
- GEYER, O.F. (1973) Das präkretazische Mesozoikum von Kolumbien. *Geol. Jahrbuch B*, **5**, 1–155.
- GILLCRIST, R., COWARD, M. & MUGNIER, J.-L. (1987) Structural inversion and its controls: examples from the Alpine foreland and the French Alps. *Geodinam. Acta*, **1**, 5–34.
- GRACIANSKY, P.C.D., DARDEAU, G., LEMOINE, M. & TRICART, P. (1989) The inverted margin in the French Alps and foreland basin inversion. In: *Inversion Tectonics* (Ed. by M.A. Cooper & G.D. Williams), *Geol. Soc. Spec. Publ.*, **44**, 87–104.
- GRIER, M.E., SALFITY, J.A. & ALLMENDINGER, R.W. (1991) Andean reactivation of the Cretaceous Salta Rift, northwestern Argentina. *J. South Am. Earth Sci.*, **4**, 351–372.
- GUIMERA, J., ALONSO, A. & RAMON MAS, J. (1995) Inversion of an extensional-ramp basin by a newly formed thrust: the Cameros Basin (N. Spain). In: *Basin Inversion* (Ed. by J.G. Buchanan & P.G. Buchanan), *Geol. Soc. Spec. Publ.*, **88**, 433–453.
- GUPTA, S., UNDERBILL, J.R., SHARP, I.R. & GAWTHORPE, R.L. (1999) Role of fault interactions in controlling synrift sediment dispersal patterns: Miocene, Abu Alaqa Group, Suez Rift, Sinai, Egypt. *Basin Res.*, **11**, 167–189.
- HAYWARD, A.B. & GRAHAM, R.H. (1989) Some geometrical characteristics of inversion. In: *Inversion Tectonics* (Ed. by M.A. Cooper & G.D. Williams), *Geol. Soc. Spec. Publ.*, **44**, 17–39.
- HILLEY, G.E., BLISNIUK, P.M. & STRECKER, M.R. (2005) Mechanics and erosion of basement cored uplift provinces. *J. Geophys. Res., Solid Earth*, **110**, B12409, doi: 10.1029/2005JB0003704, 2005.
- HUYGHE, P. & MUGNIER, J.-L. (1995) A comparison of inverted basins of the southern North Sea and inverted structures of the external Alps. In: *Basin Inversion* (Ed. by J.G. Buchanan & P.G. Buchanan), *Geol. Soc. Spec. Publ.*, **88**, 339–353.

- INGRAM, R.L. (1954) Terminology for the thickness of stratification and parting units in sedimentary rocks. *Geol. Soc. Am. Bull.*, **65**, 937–938.
- JACKSON, J. & MCKENZIE, D. (1983) The geometrical evolution of normal fault systems. *J. Struct. Geol.*, **5**, 471–482.
- KALKOWSKY, E. (1908) Oolith und stromatolith im nord-deutschen Buntsandstein. *Z. Deut. Geol. Gesellsch.*, **60**, 68–125.
- KENDALL, A.C. & HARWOOD, G.M. (1996) Marine evaporites: arid shorelines and basins. In: *Sedimentary Environments: Processes, Facies and Stratigraphy* (Ed. by H.G. Reading), pp. 281–324. Blackwell Science, Oxford.
- KLEY, J. & MONALDI, C.R. (2002) Tectonic inversion in the Santa Barbara System of the central Andean foreland thrust belt, northwestern Argentina. *Tectonics*, **21**, 1061, doi: 10.1029/2002TC902003.
- KLEY, J., ROSSELLO, E.A., MONALDI, C.R. & HABIGHORST, B. (2005) Seismic and field evidence for selective inversion of Cretaceous normal faults, Salta rift, northwest Argentina. *Tectonophysics*, **399**, 155–172.
- KOSSOW, D., KRAWCZYK, C., MCCANN, T., STRECKER, M. & NENGENDANK, J.F.W. (2000) Style and evolution of salt pillows and related structures in the northern part of the Northeast German Basin. *Int. J. Earth Sci.*, **89**, 652–664.
- KOSSOW, D. & KRAWCZYK, C.M. (2002) Structure and quantification of processes controlling the evolution of the inverted NE-German Basin. *Mar. Petrol. Geol.*, **19**, 601–618.
- LOGAN, B.W., REZAK, R. & GINSBURG, R.N. (1964) Classification and environmental significance of algal stromatolites. *J. Geol.*, **72**, 68–83.
- LOWELL, J.D. (1995) Mechanics of basin inversion from worldwide examples. In: *Basin Inversion* (Ed. by J.G. Buchanan & P.G. Buchanan). *Geol. Soc. Lond. Spec. Publ.*, **88**, 339–353.
- MCCLAY, K.R. (1995) The geometries and kinematics of inverted fault systems: a review of analogue model studies. In: *Basin Inversion* (Ed. by J.G. Buchanan & P.G. Buchanan). *Geol. Soc. Spec. Publ.*, **88**, 97–118.
- MIALL, A. (1985) Architectural-element analysis: a new method for facies analysis applied to fluvial deposits. *Earth Sci. Rev.*, **22**, 261–238.
- MIALL, A.D. (1996) *The Geology of Fluvial Deposits: Sedimentary facies, Basin Analysis, and Petroleum Geology*. Springer, New York.
- MITRA, S. (1993) Geometry and kinematic evolution of inversion structures. *Am. Assoc. Petrol. Geol. Bull.*, **77**, 1159–1191.
- MONALDI, C.R., SALFITY, J.A. & KLEY, J. (2008) Preserved extensional structures in an inverted Cretaceous rift basin, northwestern Argentina: outcrop examples and implications for fault reactivation. *Tectonics*, **27**, TC1011, doi: 10.1029/2006TC001993.
- MORA, A., PARRA, M., STRECKER, M.R., KAMMER, A., DIMATÉ, C. & RODRÍGUEZ, F. (2006) Cenozoic contractional reactivation of Mesozoic extensional structures in the Eastern Cordillera of Colombia. *Tectonics*, **25**, TC2010, doi: 10.1029/2005TC001854.
- NEMCOK, M., NEMCOK, J. & WOJTASZEK, M. (2001) Reconstruction of Cretaceous rifts incorporated in the Outer West Carpathian wedge by balancing. *Mar. Petrol. Geol.*, **18**, 39–63.
- NEMEC, W. & POSTMA, G. (1993) Quaternary alluvial fans in southwestern Crete: sedimentation processes and geomorphic evolution. In: *Alluvial Sedimentation* (Ed. by M. Marzo & C. Puidgefabregas). *Int. Assoc. Sedimentol. Spec. Publ.*, **17**, 235–276.
- PARRA, M. (2000) Estratigrafía y Petrografía del Cretácico Inferior en el Parque Natural Chingaza y la Cuenca Alta del Río Guatiquía, Cundinamarca y Meta, Colombia. B.Sc. Thesis, Universidad Nacional de Colombia, Bogotá.
- PATON, D.A. & UNDERHILL, J.R. (2004) Role of crustal anisotropy in modifying the structural and sedimentological evolution of extensional basins: The Gamtoos Basin, South Africa. *Basin Res.*, **16**, 339–359.
- PRÖSSER, S. (1993) Rift-related linked depositional systems and their seismic expression. In: *Tectonics and Seismic Sequence Stratigraphy* (Ed. by G.D. Williams & A. Dobb). *Geol. Soc. Spec. Publ.*, **71**, 35–66.
- READING, H.G. & COLLINSON, J.D. (1996) Clastic coasts. In: *Sedimentary Environments: Processes, Facies and Stratigraphy* (Ed. by H.G. Reading), pp. 154–231. Blackwell Science, Oxford.
- RIDING, R. (2000) Microbial carbonates: the geological record of calcified bacterial-algal mats and biofilms. *Sedimentology*, **47**, 179–214.
- RINCÓN, A. & TÁMARA, J. (2005) La Falla de Mirados y su significado para la sedimentación del Titoniano-Neocomiano (Vilavencio, Colombia). B.Sc. Thesis, Universidad Nacional de Colombia, Bogotá.
- ROBERTS, A.M. & YIELDING, G. (1991) Deformation around basin-margin faults in the North Sea/mid-Norway rift. In: *The Geometry of Normal Faults* (Ed. by A.M. Roberts, G. Yielding & B. Freeman). *Geol. Soc. Spec. Publ.*, **56**, 61–78.
- ROBERTS, A.M., YIELDING, G. & BADLEY, M.E. (1993) Tectonics and bathymetric controls on stratigraphic sequences within evolving half-graben. In: *Tectonics and Seismic Sequence Stratigraphy* (Ed. by G.D. Williams & A. Dobb). *Geol. Soc. Spec. Publ.*, **87**–121.
- ROEDER, D. & CHAMBERLAIN, R.L. (1995) Eastern Cordillera of Colombia: Jurassic–Neogene crustal evolution. In: *Petroleum Basins of South America* (Ed. by A.J. Tankard, S.R. Suarez & H.J. Welsink). *Am. Assoc. Petrol. Geol. Memoir*, **62**, 633–645.
- ROESSNER, S. & STRECKER, M.R. (1997) Late Cenozoic tectonics and denudation in the Central Kenya Rift: quantification of long-term denudation rates. *Tectonophysics*, **278**, 83–94.
- RUST, B. & KOSTER, E. (1984) Coarse alluvial deposits. In: *Facies Models, Geoscience Canada Reprint Series, 1*. (Ed. by R. Walker). Geological Association of Canada, Toronto.
- SARMIENTO-ROJAS, L.F., VAN WESS, J.D. & CLOETINGH, S. (2006) Mesozoic transtensional basin history of the Eastern Cordillera, Colombian Andes: inferences from tectonic models. *J. South Am. Earth Sci.*, **21**, 383–411.
- SEYFERTH, M. & HENK, A. (2006) A numerical sandbox: high resolution distinct element models of half-graben formation. *Int. J. Earth Sci.*, **95**, 189–203.
- SHANMUGAM, G. (1997) The Bouma sequence and the turbidite mind set. *Earth-Sci. Rev.*, **42**, 201–229.
- SINCLAIR, I.K. (1995) Transpressional inversion due to episodic rotation of extensional stresses in the Jeanne d'Arc Basin, offshore Newfoundland. In: *Basin Inversion* (Ed. by J.G. Buchanan & P.G. Buchanan). *Geol. Soc. Spec. Publ.*, **88**, 249–271.
- Stibane, F.R., ed. (1968) *Zur Geologie von Kolumbien, Südamerika: Das Quetame- und Garzon-Massiv*. Geotektonische Forschungen. E. Schweizerbart, Stuttgart.
- TEIXELL, A., ARBOLEYA, M.-L., JULIVERT, M. & CHARROUD, M. (2003) Tectonic shortening and topography in the central High Atlas (Morocco). *Tectonics*, **22**, 1051, doi: 10.1029/2002TC001460.
- THOMAS, D.W. & COWARD, M.P. (1995) Late Jurassic–Early Cretaceous inversion of the northern East Shetland Basin, northern North Sea. In: *Basin Inversion* (Ed. by J.G. Buchanan & P.G. Buchanan). *Geol. Soc. Spec. Publ.*, **88**, 275–306.

- TRUDGILL, B. & CARTWRIGHT, J. (1994) Relay-ramp forms and normal-fault linkages, Canyonlands National Park, Utah. *Geol. Soc. Am. Bull.*, **106**, 1143–1157.
- TUCKER, M.E. & WRIGHT, V.P. (1990) *Carbonate Sedimentology*. Blackwell Scientific Publications, Oxford.
- ULIANA, M.A., ARTEAGA, M.E., LEGARRETA, L., CERDÁN, J.J. & PERONI, G.O. (1995) Inversion structures and hydrocarbon occurrence in Argentina. In: *Basin Inversion* (Ed. by J.G. Buchanan & P.G. Buchanan. *Geol. Soc., Lond.* **88**, 211–233.
- ULLOA, C. & RODRÍGUEZ, E. (1979) Geología del Cuadrángulo K12, Guateque. *Bol. Geol. Ingeom.*, **22**, 3–55.
- UNDERHILL, J.R. & PATERSON, S. (1998) Genesis of tectonic inversion structures: seismic evidence for the development of key structures along the Purbeck-Isle of Wight disturbance. *J. Geol. Soc.*, **155**, 975–992.
- WALSH, J.J., BAILEY, W.R., CHILDS, C., NICOL, A. & BONSON, C.G. (2003) Formation of segmented normal faults: a 3-D perspective. *J. Struct. Geol.*, **25**, 1251–1262.
- WALSH, J.J., NICOL, A. & CHILDS, C. (2002) An alternative model for the growth of faults. *J. Struct. Geol.*, **24**, 1669–1675.
- WARREN, J.K. & KENDALL, C.G.S.C. (1985) Comparison of sequences formed in marine sabkha (subaerial) and salina (subaqueous) settings: modern and ancient. *Am. Assoc. Petrol. Geol. Bull.*, **69**, 1013–1023.
- WILLIAMS, G.D., POWELL, C.M. & COOPER, M.A. (1989) Geometry and kinematics of inversion tectonics. In: *Inversion Tectonics* (Ed. by M.A. Cooper & G.D. Williams, *Geol. Soc. Spec. Publ.*, **44**, 3–15.
- WITHJACK, M.O., ISLAM, Q.T. & LA POINTE, P.R. (1995) Normal faults and their hanging-wall deformation: an experimental study. *Am. Assoc. Petrol. Geol. Bull.*, **79**, 1–18.
- YAMADA, Y. & McCLAY, K.R. (2004) Analog modeling of inversion thrust structures: experiments of 3D inversion structures above listric fault systems. In: *Thrust Tectonics and Petroleum Systems* (Ed. by K.R. McClay), *Am. Assoc. Petrol. Geol. Memoir*, **82**, 276–302.

Manuscript received 13 April 2007; Manuscript accepted 15 May 2008.